Reinterpretation of the ATLAS Search for Top Squarks Decaying to Tau Sleptons in Terms of Third Generation Scalar Leptoquarks

Reinterpretation der ATLAS-Suche nach Top-Squarks mit Zerfällen in Tau-Sleptonen als Suche nach skalaren Leptoquarks der dritten Generation

Masterarbeit der Fakultät für Physik
der
Ludwig-Maximilians-Universität München

vorgelegt von

Alexander Mario Lory

geboren in Zürich

München, den 09.05.2018

Contents

Chapter 1

Introduction

The Standard Model (SM) of particle physics is in good agreement with most experimental data and successfully describes the fundamental strong, weak and electromagnetic interactions. With the observation of the Higgs boson in 2012 at the LHC, the last missing piece of the SM was discovered. But the SM leaves several questions unanswered. Especially, it lacks a description of gravity and dark matter. Moreover, the observed mass of the Higgs boson is surprisingly low, such that the quantum corrections to its mass need a high amount of fine-tuning. There are also experimental hints of discrepancies. Indeed, measurements on the physics of B-hadrons observe deviations from the SM prediction. This suggests that there is physics that goes beyond the Standard Model (BSM). Many extensions of the SM try to explain the generational structure of the SM and the symmetries between the charges of leptons and quarks. They often predict new states called leptoquarks (LQs), which carry both lepton and baryon number. These might be in reach of the Large Hadron Collider and they can potentially explain the anomalies observed in the physics of B-hadrons.

Other BSM extensions predict a symmetry between bosons and fermions, called supersymmetry. This symmetry is theoretically and phenomenologically well motivated and very popular amongst particle physicists, which devote a lot of work to search for it. As a consequence, the set of all searches for supersymmetry covers a wide range of possible final states. But the phase spaces in which searches for supersymmetry are performed are often also sensitive to other BSM models.

In this work, we take advantage of this by reinterpreting the ATLAS search for top squarks decaying to tau sleptons in 36.1 fb pp collisions at 13 TeV [1] in terms of scalar leptoquarks of the third generation (LQ_3). We obtain strong limits for models with intermediate values of β, which predict the mixed final state $t\tau b\nu$. We obtain the currently[1] highest mass-reach of the ATLAS experiment for pair produced up-type LQ_3 with $\beta \simeq 0.6$.

This reinterpretation also illustrates the problem of signal contamination in auxiliary background measurements. We discuss the implications and propose a method to avoid it.

[1] As of May 2018.

Chapter 2

Theoretical Foundation

2.1 The Standard Model of Particle Physics

2.1.1 Overview

The standard model (SM) of particle physics [2, 3, 4] is an ad-hoc description of strong, weak and electromagnetic interactions in the framework of quantum field theory, which describes the mechanics of relativistic fields.

The model is based on the principle of local gauge invariance, applied to the symmetry group $G = \mathrm{SU}(3)_c \times \mathrm{SU}(2)_L \times \mathrm{U}(1)_Y$, such that the resulting gauge fields mediate interactions between fermionic fields representing matter. The gauge fields act on fermionic fields if the fermions carry the corresponding charge. For $\mathrm{SU}(3)_c$ the charge is color, for $\mathrm{SU}(2)_L$ it is weak isospin and for $\mathrm{U}(1)_Y$ hypercharge. The only (elementary) scalar field of the theory, the Higgs field, has a non-vanishing vacuum expectation value. As a result, the dynamics around the ground state do not exhibit all symmetries of G. The electroweak symmetry $\mathrm{SU}(2)_L \times \mathrm{U}(1)_Y$ is broken such that bosons mediating weak interactions, i.e. the $W^\pm$ bosons and the Z boson, are massive. The photon γ remains massless. The Higgs field is also responsible for the generation of fermion masses, through its Yukawa couplings to the fermionic fields.

The matter content is divided into quarks and leptons. Quarks are the femions with color charge. For each quark flavor (u, d, c, s, t, b), there is one color triplet, on which the strong force acts. The remaining fermions are leptons and are $\mathrm{SU}(3)_c$ singlets, i.e., they do not interact strongly.

The weak force only acts on left-handed particles. Therefore, left- and right-handed components are to be treated separately and all right-handed fermions are $\mathrm{SU}(2)_L$ singlets. The charged, left-handed leptons form weak isopsin doublets with the neutral, left-handed neutrinos. There is one $\mathrm{SU}(2)_L$ doublet for each lepton flavor:

$$\begin{pmatrix} \nu_e \\ e_L \end{pmatrix}, \begin{pmatrix} \nu_\mu \\ \mu_L \end{pmatrix}, \begin{pmatrix} \nu_\tau \\ \tau_L \end{pmatrix}.$$

Left-handed quarks also form weak isopsin doublets:

$$\begin{pmatrix} u_L \\ d_L \end{pmatrix}, \begin{pmatrix} c_L \\ s_L \end{pmatrix}, \begin{pmatrix} t_L \\ b_L \end{pmatrix}.$$

We recognize that there are three generations of fermions (ν_i, e_i, u_i, d_i) with $i = 1, 2, 3$, which have the same quantum numbers, but different masses. Figure 2.1 summarizes the particle content and figure 2.2 the possible interactions in the SM. The mass eigenstates, which are the observable fields, of d, s and b are not the $\mathrm{SU}(2)_L$ partners of u, c and t, respectively. But we can write the isospin doublets in terms of mass eigenstates as

$$\begin{pmatrix} u \\ d' \end{pmatrix}, \begin{pmatrix} c \\ s' \end{pmatrix}, \begin{pmatrix} t \\ b' \end{pmatrix}, \qquad \text{with} \begin{pmatrix} d' \\ s' \\ b' \end{pmatrix} = V_{CKM} \begin{pmatrix} d \\ s \\ b \end{pmatrix},$$

where V_{CKM} is the Cabibbo-Kobayashi-Maskawa matrix. Thus, weak charged currents can involve quark flavors of different generations. Weak neutral currents (and also strong and electromagnetic currents), are flavor diagonal.

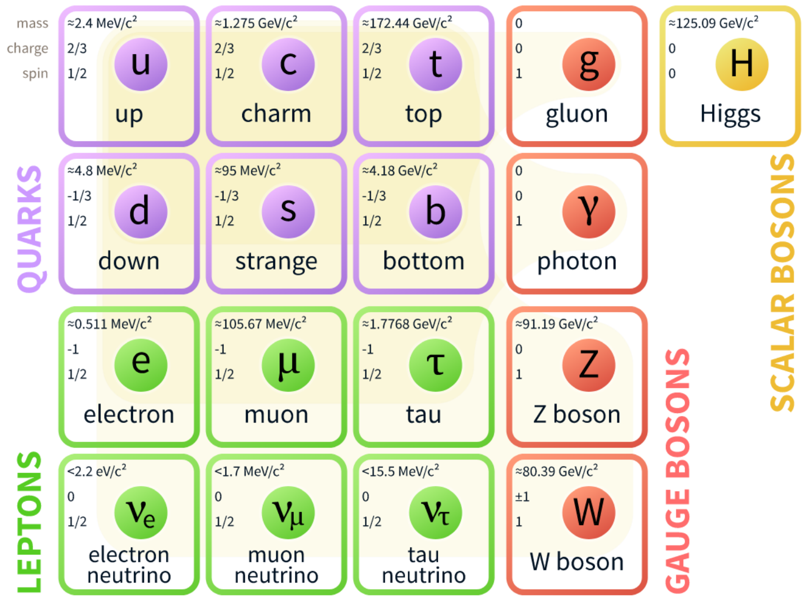

Figure 2.1: Particle content of the standard model [5].

2.1.2 Shortcomings of the Standard Model

Although the SM successfully describes experimental data, it remains mysterious from a theoretical point of view. Indeed, several intriguing questions remain unanswered in the SM: Why has nature chosen the symmetry group G? Why does the weak interaction act only on left-handed fermions? Why are there three generations of fermions and why is the charge of the electron exactly three times that of the down quark? The SM has 19 free parameters that need to be determined experimentally. But for a fundamental theory, we would like to have as few as possible.

Grand unified theories (GUTs) can reduce the number of parameters of the model. They state that all elementary interactions emerge from the same fundamental interaction in a gauge group of higher symmetry. This higher symmetry is hidden through spontaneous symmetry breaking in a similar wat that the electroweak symmetry is hidden in the SM. As we will see, the unification of coupling constants, which would take place at around 10^{16} GeV, is only exact with supersymmetry. Anyways, if we want to answer some of the questions above, BSM physics is needed.

The SM is also in tension with other fields of physics. Indeed, we know from cosmological and astrophysical observations, that there is more than ordinary matter in the universe. Only about a fifth of the matter content of the universe can be attributed to particles from

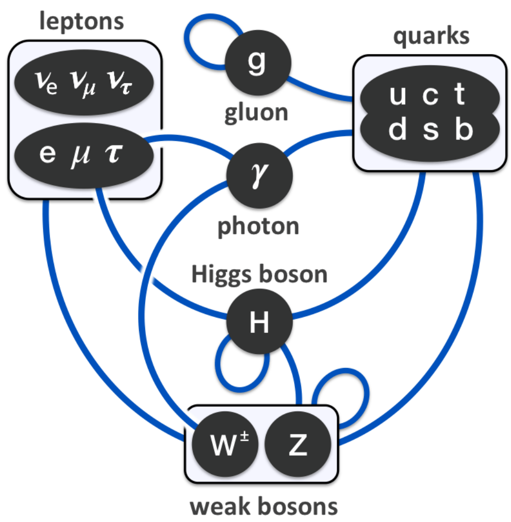

Figure 2.2: Possible interactions in the standard model [6]. The gauge bosons (gluon g, weak bosons $W^{\pm}$ and Z and photon γ) interact with all particles carrying the corresponding charge. The photon does not interact with himself, as it has no electromagnetic charge. The Higgs boson (H) couples to any massive particle.

the SM. The observation of rotations of galaxies, of gravitational lenses and of large scale structures [7] suggest that there is "dark" matter. The most prominent explanation for dark matter is the presence of weakly interacting massive particles (WIMPs). In the SM, the neutrino is the only particle which exclusively interacts weakly, but it is too light to be a viable WIMP candidate.
Moreover, observations of the red-shift in supernovae of types which have very uniform luminosities, indicate that the expansion of the universe is accelerating. A new form of energy is needed to explain this. Observation of the fluctuations in the cosmic microwave background also indicates that baryonic and dark matter only make up about 30% of the energy content of the universe [8].
Finally, the SM does not describe gravity. But we have to find a way to treat gravity at the Planck scale (10^{19} GeV), where quantum effects become important. These observations and considerations are further arguments that indicate that the SM is a low-energy approximation, only valid up to some scale Λ.

If there is new physics at some scale Λ, then the Higgs mass is not natural. In quantum field theory, processes are described by perturbation theory. Any tree-level process receives higher order corrections. Masses receive corrections to their bare mass, as they are constantly interacting with the surrounding fields. The mass of the Higgs boson is a special case. Since it is a scalar, it receives quadratically divergent contributions to its mass and therefore, it is very sensitive to quantum corrections. Hence, the "outcome" of its physical mass, after corrections, should naturally be of the order of the heaviest particle of the theory. We observe the Higgs mass to be about 125 GeV, but expect new physics at the scale of unification (10^{16} GeV) or at the Planck scale (10^{19} GeV). In the presence of such a high hierarchy of scales, the contributions to the Higgs mass must be extremely fine-tuned in order to explain such a light observable mass.

2.2 Supersymmetry

Supersymmetry [3, 4] (SUSY) is a symmetry between fermions and bosons. The fermionic operator Q turns fermions into bosons and vice-versa:

$$Q|f\rangle = |b\rangle$$
$$Q|b\rangle = |f\rangle,$$

where $|f\rangle$ is a fermionic and $|b\rangle$ a bosonic state. As a consequence, the spin varies by $1/2$. All other quantum numbers of the particle stay the same. Some examples of its application are shown in table 2.1.

Particle	SUSY partner
lepton ($1/2$)	slepton (0)
quark ($1/2$)	squark (0)
gauge boson (1)	gaugino ($1/2$)
Higgs boson (0)	higgsino ($1/2$)
graviton (2)	gravitino ($3/2$)

Table 2.1: Some particles and the particle obtained after applying the fermionic operator Q. The spins of the particles are shown in brackets.

2.2.1 The answer to many questions

One of the beauty of SUSY is that it can solve many shortcomings of the SM:

- The quantum corrections from a fermionic and a bosonic state with otherwise same quantum numbers cancel out. The top quark, with his strong Yukawa coupling, induces the highest corrections to the mass of the Higgs boson. Therefore, if the SUSY partner of the top quark has a low mass, such that the cancellation starts at sufficiently low energies, the Higgs mass is natural.

- The coupling constants of the SM are only constant at lowest order perturbation theory. When we consider higher order corrections, the couplings depend on the energy scale. The SM predicts that the values of the coupling strengths get close to each other at the unification scale (10^{16}GeV), but they never merge, as can be seen on figure 2.3. This is a disappointment for GUTs. But the running of the couplings is modified in the presence of SUSY and the couplings can therefore be unified, if SUSY corrections become important at the TeV scale. Again, the TeV scale is important. If the corrections only contribute at higher energies, the coupling strengths do not merge.

- A lot of SUSY models have excellent candidates for dark matter, like the neutralino or the gravitino.

- The unification with gravity is easier. One reason being that a theory including SUSY is protected against quadratic divergences, even up to the Planck scale. Moreover, the fermionic operators of SUSY are related to space-time symmetries with the anicommutation relation $\{Q, \overline{Q}\} \propto P^{\mu}$, where P^{μ} is the four-momentum generator of space-time translations. This gives a new tool that can be used to implement gravity in particle physics.

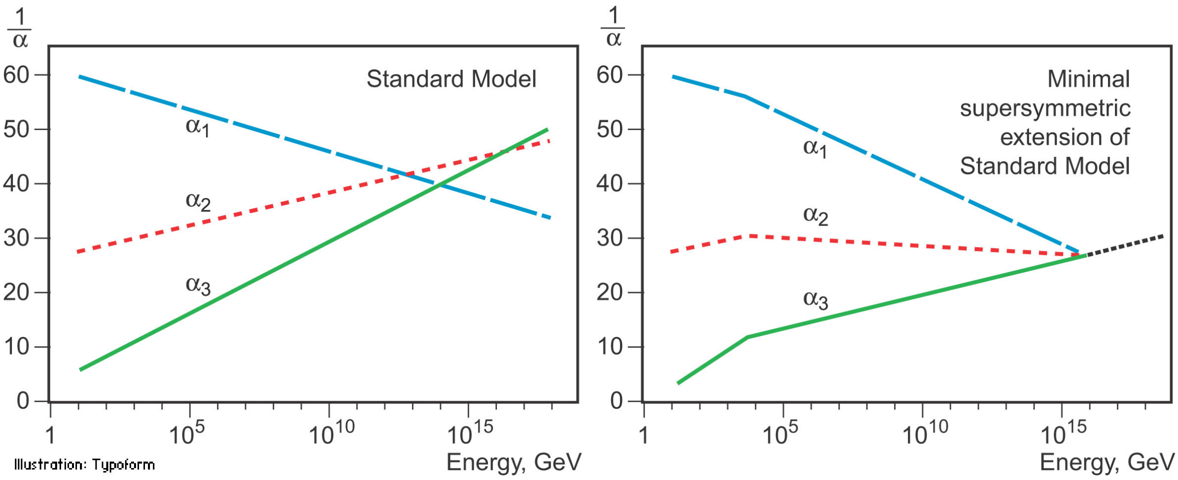

Figure 2.3: Evolution of the coupling strengths of electromagnetic (α_1), weak (α_2) and strong interactions (α_3) with the energy scale as predicted by the SM (left) and with SUSY (right) [9].

2.2.2 The minimal supersymmetric standard model

The minimal supersymmetric standard model (MSSM) is the supersymmetrized version of the SM with a minimal number of new particles. It is required to solve the problem of naturalness of the Higgs mass and to be consistent with phenomenology. I.e., the following constraints have to be fulfilled:

- The gauge group is that of the standard model and the electroweak symmetry is broken.
- Since we do not observe SUSY particles with the same masses as their SM partners, also SUSY has to be broken. But if we want SUSY to cancel quadratic divergences, relations between couplings still have to hold. Therefore, SUSY has to be broken explicitly in a way that forbids the reappearance of quadratic divergences. This is called *soft* SUSY breaking.
- Lepton (L) and baryon (B) numbers have to be conserved. But unlike in the SM, SUSY couplings can in general lead to L and B violations. This is avoided by introducing an additional symmetry: R-parity. It is characterized by the multiplicative quantum number

  $$P_R = (-1)^{3(B-L)+2s},$$

  where s is the spin. All SM particles have $P_R = 1$ and their SUSY partners have $P_R = -1$. As a consequence, SUSY particles can only be created in pairs and the lightest SUSY particle (LSP) is stable. If the LSP only interacts weakly, it is a good WIMP candidate for dark matter. Its signature at colliders is missing energy, since it does not interact with the detector.

The new particles appearing in the MSSM are shown in table 2.2, together with the SM Higgs boson (h^0) in the column listing the mass eigenstates. It should be noted that the Higgs sector has been extended, since two Higgs doublets are needed to prevent anomalies in the electroweak gauge symmetry and to supply the necessary Yukawa couplings. These two complex doublets form eight degrees of freedom, from which three give mass to the weak gauge bosons after electroweak symmetry breaking. The remaining five manifest as Higgs bosons, where three are neutral (h^0, H^0 and A^0) and two are charged ($H^\pm$). The subscripts L and

Name	Spin	Gauge eigenstates	Mass eigenstates
Higgs bosons	0	H_u^0,H_d^0,H_u^+,H_d^-	h^0,H^0,A^0,$H^\pm$
squarks	0	$\tilde{u}_L$,$\tilde{u}_R$,$\tilde{d}_L$,$\tilde{d}_R$ $\tilde{c}_L$,$\tilde{c}_R$,$\tilde{s}_L$,$\tilde{s}_R$ $\tilde{t}_L$,$\tilde{t}_R$,$\tilde{b}_L$,$\tilde{b}_R$	same same $\tilde{t}_1$,$\tilde{t}_2$,$\tilde{b}_1$,$\tilde{b}_2$
sleptons	0	$\tilde{e}_L$,$\tilde{e}_R$,$\tilde{\nu}_e$ $\tilde{\mu}_L$,$\tilde{\mu}_R$,$\tilde{\nu}_\mu$ $\tilde{\tau}_L$,$\tilde{\tau}_R$,$\tilde{\nu}_\tau$	same same $\tilde{\tau}_1$,$\tilde{\tau}_2$,$\tilde{\nu}_\tau$
neutralinos	1/2	$\tilde{B}^0$,$\tilde{W}^0$,$\tilde{H}_u^0$,$\tilde{H}_d^0$	$\tilde{\chi}_1^0$,$\tilde{\chi}_2^0$,$\tilde{\chi}_3^0$,$\tilde{\chi}_4^0$
charginos	1/2	$\tilde{W}^\pm$,$\tilde{H}_u^+$,$\tilde{H}_d^-$	$\tilde{\chi}_1^\pm$,$\tilde{\chi}_2^\pm$
gluino	1/2	$\tilde{g}$	same
gravitino	3/2	$\tilde{G}$	same

Table 2.2: Particle content of the MSSM. Adapted from [10].

R refer to the chirality of their SM partners. As in the SM, observable mass eigenstates do not always coincide with the gauge eigenstates. The SUSY partners of neutral gauge bosons mix with neutral higgsinos to form neutralinos $\tilde{\chi}^0_{1,2,3,4}$ and the SUSY partners of the charged gauge bosons mix with the charged higgsinos to form charginos $\tilde{\chi}^\pm_{1,2}$. The SUSY partners of the heaviest quarks and leptons also mix. The mass spectrum of the MSSM is defined by the parameters of the model. If we choose the parameters such that the naturalness problem of the Higgs mass should be solved, constraints appear on the masses of sparticles, especially the ones closely related to the Higgs boson, namely higgsinos and the SUSY partners of the heaviest fermions. These should be light for low fine-tuning [10].

2.3 Leptoquarks

The symmetries between leptons and quarks, i.e., the fact that the charges of quarks are multiples of 1/3 of the charge of electrons and the fact that there are three generations of quarks and leptons, can be seen as natural if leptons and quarks are related on a fundamental level. Theories which account for such a relation often predict new states having both lepton and baryon number called leptoquarks. Leptoquarks have attracted recent interest due to discrepancies between SM expectations and observations in the physics of B-hadrons measured by Babar [11], Belle [12] and LHCb [13]. For example, LHCb measured a 2.6σ deviation from the SM prediction of the ratio of branching ratios $\frac{\mathrm{BR}(\overline{B}\to\overline{K}\mu^+\mu^-)}{\mathrm{BR}(\overline{B}\to\overline{K}e^+e^-)}$. The collected data can be explained with the characteristic lepton-quark coupling of leptoquarks [14]. In the SM, both of these $\overline{B}$ decays are possible with at least 4 weak vertices, as shown in figure 2.4 for $\overline{B}\to\overline{K}\mu^+\mu^-$. This decay is very sensitive to contributions from tree level processes involving leptoquarks. An example is shown on the same figure.

2.3.1 Theoretical motivation

Leptoquark properties, like their quantum numbers and masses, depend on the proposed model and give rise to a rich phenomenology. In the following, we will describe some of the most popular models involving leptoquarks and the different types of predicted leptoquarks.

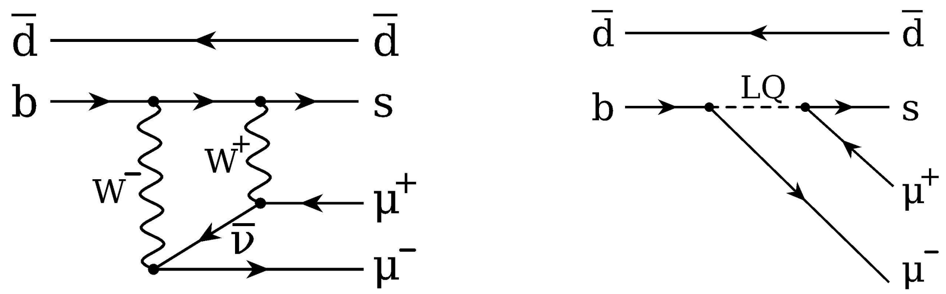

Figure 2.4: Diagrams for the decay $\overline{B}\to\overline{K}\mu^+\mu^-$ through weak interactions (left) and with LQ interaction (right).

Pati-Salam Leptoquarks had their first appearance in the Pati-Salam model [15] which tries to explain why quarks and leptons are so similar, and at the same time why left- and right-handed states are so different. This model proposes that quarks come in four colors instead of the usual three. The three familiar colors represent baryonic matter and the fourth color represents the lepton number. Quarks and leptons are grouped together in fermionic multiplets like

$$\begin{pmatrix} u_1 \\ u_2 \\ u_3 \\ \nu \end{pmatrix}_i , \quad \begin{pmatrix} d_1 \\ d_2 \\ d_3 \\ \ell \end{pmatrix}_i , \quad i = 1,2,3$$

where the subscripts 1,2,3 refer to color and i to the three generations of fermions. The gauge group of the model is $\mathrm{SU}(4)\times\mathrm{SU}(2)_L\times\mathrm{SU}(2)_R$ and generates the strong, the weak and the electromagnetic interactions by spontaneous symmetry breaking if the

Higgs field has a vacuum expectation value. As a consequence, gauge bosons carrying both lepton and baryon number must exist. Their mass would be at the scale of SU(4) symmetry breaking, which can be around 10^5 GeV [16].

Grand Unified Theories (GUTs) The model of Pati-Salam is sometimes called a "petite" unified theory as its gauge group is not a simple Lie group and interactions are not unified (several coupling strengths are needed). In contrast, in GUTs, like SU(5) [17] or SO(10) [18], the strong, the weak and the electromagnetic interactions are assumed to emerge from the same fundamental interaction. Leptons and quarks also share multiplets and again, spontaneous symmetry breaking hides the higher symmetry. Additional gauge bosons, carrying both lepton and baryon number are expected at the GUT scale in the order of 10^{15} GeV [19, 20]. They violate lepton and baryon number conservation, which, as we will see, can induce the decay of the proton.

Composite models In order to reduce the number of elementary particles and parameters of the SM and to explain the similarities between quarks and leptons, one could consider a scenario in which fermions are not fundamental, but composed of so-called preons [21]. In that case, fermions, and other standard model particles, would be bound states of preons, in a similar way that hadrons are bound states of quarks. Composite models can also explain the structure of generations, as the second and third generations would be higher excitations of the first generation, which makes them more massive while the charges stay the same. In composite models, leptoquarks appear as a specific arrangement of preons. They would have spin 1 or 0 and could be either heavy resonances or light pseudo-Nambu-Goldstone bosons with masses of a few hundred GeV, if the preons exhibit a broken approximate symmetry [22] [23].

Technicolor Technicolor models propose an alternative to the standard model's elementary scalar for the mass generation of elementary particles [20]. A new strong gauge interaction is introduced which couples to new fermions called technifermions. The chiral symmetry of the technifermions is spontaneously broken, which generates the masses of the $W^{\pm}$ and Z bosons dynamically. In extended technicolor models, which also include a mechanism to generate the masses of fermions, TeV-scale leptoquarks are expected as bound states composed of technifermions [24].

Supersymmetry We have seen that introducing R-parity in supersymmetric models ensures lepton and baryon number conservation. This forbids proton decay and gives good candidates for dark matter. But without R-parity, SUSY can still solve the problem of naturalness of the Higgs mass if the lightest squarks have masses at the TeV scale. If Yukawa couplings between fermions and squarks are allowed, these scalar particles would have the properties of leptoquarks [25].

2.3.2 Phenomenology

Couplings between quarks and leptons allow for a variety of processes that would not be allowed or only allowed at higher orders in the SM. We will discuss some of these processes here in order to determine what realistic leptoquark states we can encounter at colliders. We will then be able to compare these to the states predicted by the simplified models we use for the search of third generation scalar leptoquarks.

Chirality For a leptoquark to be sufficiently light to be relevant for collider searches, it has to be chiral. We come to this conclusion by examining low energy experiments, like the measurement of the magnetic moment of the muon. The SM interaction of a muon with a magnetic field can be illustrated by the top-left and top-right Feynman diagrams of figure 2.5, which show the lowest order and a higher order process of a photon interacting with a muon. If a leptoquark couples to a quark and a left-handed muon with strength λ_L, but also to a quark and a right-handed muon with strength λ_R, the bottom diagram in figure 2.5 would significantly contribute to the magnetic moment of the muon. This means that for light leptoquarks either λ_L or λ_R has to be close to 0 [26].

Moreover, a leptoquark that couples to ue_R^- with strength λ_R and to $d\nu_L$ with strength λ_L can give a large contribution to the process $\pi^+ \to e^+\overline{\nu}_e$. In the SM, the electronic pion decay $\pi^+ \to e^+\nu_e$ is allowed, but suppressed by helicity. Since we do not measure an excess of this decay mode, we conclude that light leptoquarks must be chiral [26].

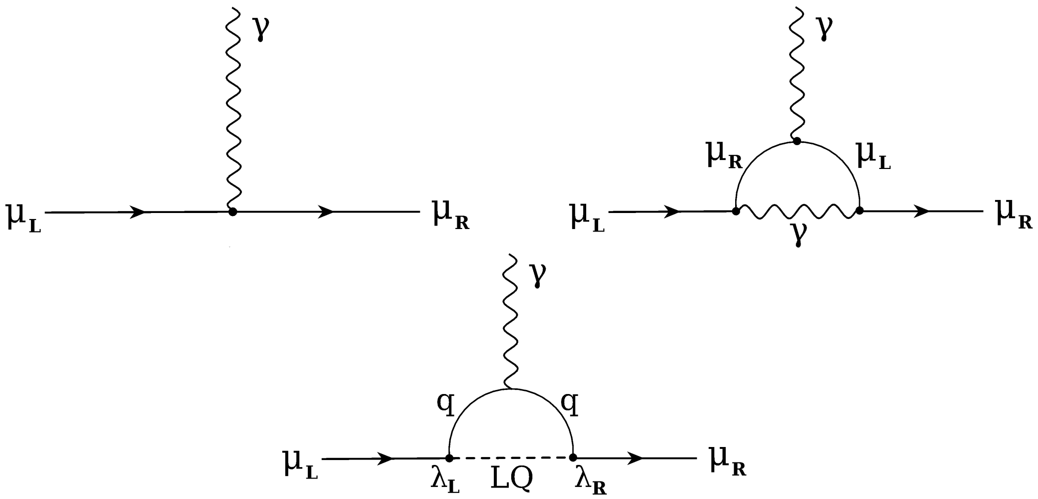

Figure 2.5: Diagrams of the interaction of a muon with a magnetic field with the lowest order process of the SM (top-left), a loop correction (top-right) and a hypothetical contribution from a non-chiral leptoquark (bottom).

Baryon and lepton number conservation The proton is stable in the SM. Leptoquarks that, in addition to the quark lepton coupling, also couple to two quarks, like in SU(5), can induce the decay of the proton, through, for example, the process shown in figure 2.6. This process violates baryon and lepton number conservation. In this decay channel, the lifetime of the proton was measured to be larger than 10^{34} years [27]. So again, this decay has either to be suppressed by a very large mass of the leptoquark, or the theory has to conserve lepton and baryon number.

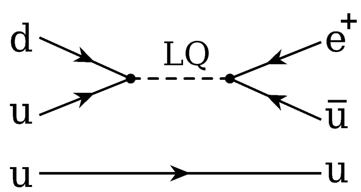

Figure 2.6: Diagram of the decay of the proton with diquark and quark-lepton couplings mediated by a leptoquark.

Inter-generational coupling The SM does not allow for flavor changing neutral currents (FCNC) at tree level. However, if a leptoquark interaction vertex accepts fermions from different generations, it can contribute in a variety of FCNC and lepton number violations [28]. Moreover, FCNCs can also occur if the same leptoquark can couple to pairs of fermions from different generations (even if only one generation is involved at each vertex). This could, for example, induce the decay $K \to e\mu$, through the process shown in figure 2.7, which is a FCNC and violates lepton family number conservation. This suggests that leptoquarks belong to a certain generation themselves and couple only to fermions of that same generation [26].

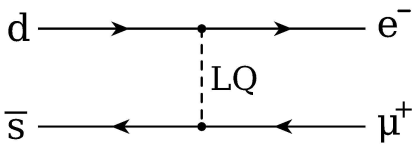

Figure 2.7: Diagram for the decay $\overline{K} \to e^+\mu^-$ with LQ interaction.

Realistic leptoquark states should also be compatible with the SM. Therefore, their couplings must be invariant under the SM gauge group and be renormalizable. All possible scalar, chiral leptoquark states that fulfill these conditions are listed in table 2.3. The branching fraction of their decay into a charged lepton and a quark is given by β, in the limit of heavy leptoquark masses or massless decay products. β can have values of 0, 1 or $1/2$. A fermion number (F = 3B + L) is assigned to leptoquarks. It is conserved, even if we would allow for lepton and baryon number violations. Leptoquarks are all color triplets, which means that they can be produced copiously at hadron colliders.

Leptoquarks can also have spin 1. The main difference, for our purpose (the search at colliders), between scalar and vector leptoquarks, is that gauge couplings of the scalar leptoquarks are set by their quantum numbers, which is not the case for vector leptoquarks. Hence, models including vector leptoquarks have to consider an additional parameter, which, besides the mass of the leptoquark, determines the production cross-section. In this work we only consider scalar leptoquarks.

Leptoquarks can be produced in pairs at hadron colliders through the processes shown in figure 2.8, which include gluon fusion ($gg \to \mathrm{LQ}\overline{\mathrm{LQ}}$), quark antiquark annihilation ($q\bar{q} \to \mathrm{LQ}\overline{\mathrm{LQ}}$) and lepton exchange. For scalar leptoquarks at the LHC, lepton exchange can be neglected [29] and the leading order production cross-sections for gluon fusion and quark antiquark annihilation are given by [19]:

$$
\begin{aligned}
\sigma_{\mathrm{LO}}(q\bar{q} \to \mathrm{LQ}\overline{\mathrm{LQ}}) &= \frac{2\alpha_s^2\pi}{27s}\zeta^3 \quad \text{and} \\
\sigma_{\mathrm{LO}}(gg \to \mathrm{LQ}\overline{\mathrm{LQ}}) &= \frac{\alpha_s^2\pi}{96s} \times \left[\zeta(41-31\zeta^2) + (18\zeta^2-\zeta^4-17)\log\frac{1+\zeta}{1-\zeta}\right],
\end{aligned}
$$

respectively. α_s is the strong coupling, $\sqrt{s}$ the invariant energy of the parton subprocess and $\zeta = \sqrt{1 - 4m_{\mathrm{LQ}}^2/s}$. These cross-sections are the same as for the production of squarks, since they have the same spin and are both color triplets. It should be noted that through the Yukawa coupling, leptoquarks could also be produced singly, with associated production of a lepton. We do not consider this process here, but other analyses, like [30], specifically target this process, which allows for high mass reaches if the Yukawa coupling is strong.

LQ	F	T_3	Q_{EM}	Yukawa couplings	β
S_{1L}	2	0	$+1/3$	$(\ell^+\overline{u})_L$,$(\overline{\nu}\overline{d})_L$	$1/2$
S_{1R}	2	0	$+1/3$	$(\ell^+\overline{u})_R$	1
$\tilde{S}_{1R}$	2	$+1$	$+4/3$	$(\ell^+\overline{d})_R$	1
S_{3L}	2	$+1$	$+4/3$	$(\ell^+\overline{d})_L$	1
		0	$+1/3$	$(\ell^+\overline{u})_L$, $(\overline{\nu}\overline{d})_L$	$1/2$
		-1	$-2/3$	$(\overline{\nu}\overline{u})_L$	0
R_{2L}	0	$+1/2$	$+5/3$	$(\ell^+u)_L$	1
		$-1/2$	$+2/3$	$(\overline{\nu}u)_L$	0
R_{2R}	0	$+1/2$	$+5/3$	$(\ell^+u)_R$	1
		$-1/2$	$+2/3$	$(\ell^+d)_R$	1
$\tilde{R}_{2L}$	0	$+1/2$	$+2/3$	$(\ell^+d)_L$	1
		$-1/2$	$-1/3$	$(\overline{\nu}d)_L$	0

Table 2.3: Possible scalar, chiral leptoquark states assuming renormalizable diagonal couplings invariant under the SM gauge interactions [26]. The nomenclature is S (R) for scalar leptoquarks with fermion number $F = 3B + L = 2$ (0). Subscripts indicate the chirality of the Yukawa coupling and weather the leptoquarks are singlets (1), doublets (2) or triplets (3) under $SU(2)_L$. T_3 is the third component of the weak isospin and Q_{EM} is the electromagnetic charge. For the possible Yukawa couplings, u (d) can be any up-type (down-type) quark (but always pair-wise from the same generation). β is the branching ratio of the decay into a charged lepton in the limit of high leptoquark masses.

2.3.3 Simplified models

In order to search for third generation leptoquarks LQ_3, we consider two simplified models, which cover all possible Yukawa couplings of the third generation[1]. In these, the leptoquarks have charges of $Q_{\mathrm{EM}} = -1/3$ and $+2/3$, for down (d) and up-type (u) leptoquarks, respectively. For this, we consider the interaction Lagrangian from [31] for the Yukawa couplings:

$$\mathcal{L}^{\mathrm{d}} = \lambda_\ell(\sqrt{\eta_L}\,\overline{u}_R\ell_L^+ + \sqrt{\eta_R}\,\overline{u}_L\ell_R^+)\ell_q + \lambda_\nu\overline{d}_R\widetilde{\nu}_L^\ell\ell_q + \text{h.c.}, \tag{2.1}$$

$$\mathcal{L}^{\mathrm{u}} = \lambda_\ell(\sqrt{\eta_L}\,\overline{d}_R\ell_L^- + \sqrt{\eta_R}\,\overline{d}_L\ell_R^-)\ell_q + \lambda_\nu\overline{u}_R\nu_L^\ell\ell_q + \text{h.c.}, \tag{2.2}$$

where u, d, ℓ, ν^ℓ are the fermionic fields of up and down-type quarks and charged leptons and neutrinos and ℓ_q is the scalar field of the leptoquark. η_L and $\eta_R = (1 - \eta_L)$ are the chiralilty fractions of the charged leptons that take part in the interaction, i.e., they give the fraction of left or right-handed charged leptons coming from a leptoquark decay. Since leptoquarks should be chiral and since our analysis does not account for the helicity of the decay products, we set $\eta_L = 0$. $\lambda_\ell = \beta\lambda^2$ and $\lambda_\nu = (1-\beta)\lambda^2$ are the coupling strengths parameters to charged leptons and neutrinos, respectively. By varying the parameter β, we can probe the different leptoquark states of table 2.3. For third generation fermions, this Lagrangian describes couplings of $\mathrm{LQ}_3^{\mathrm{u}}$ to a b-quark and tau lepton or/and to a top-quark and a tau-neutrino and of $\mathrm{LQ}_3^{\mathrm{d}}$ to a b-quark and a tau-neutrino or/and to a top-quark and a tau lepton.

[1] We cover all possible Yukawa couplings if we neglect the difference between particle and antiparticle, in the sense that we do not consider the difference between e.g. a leptoquark that couples to ℓu and a leptoquark that couples to $\ell\overline{u}$. We would otherwise need additional simplified models, with different leptoquark charges.

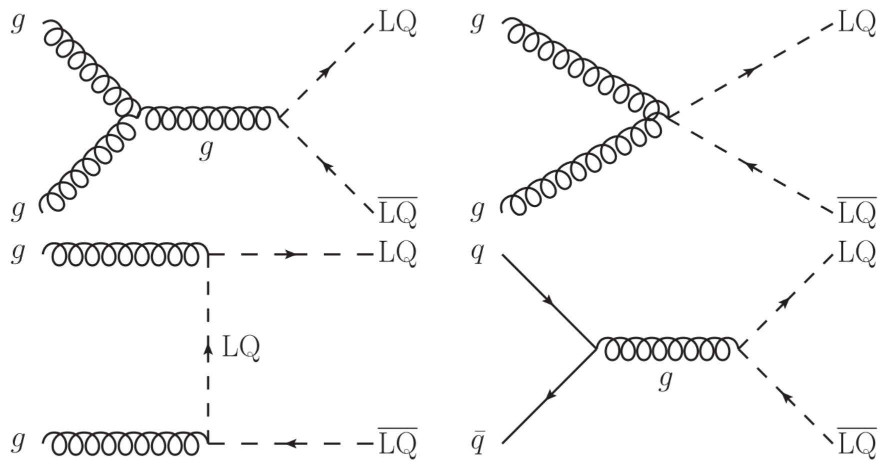

Figure 2.8: LQ pair production through gluon fusion (top), quark anti-quark annihilation (bottom-right) and lepton exchange (bottom-left)[32].

As stated before, β is the branching ratio of a leptoquark into a charged lepton, in the limit of heavy leptoquark mass or massless decay products. Therefore, for first and second generation leptoquarks, the branching ratio can be approximated by β. For the third generation and for the leptoquark masses that we will consider, it is a bad approximation, since we consider decays to the massive top quark. We can calculate the branching ratios as a function of the leptoquark mass from the ratios of the decay widths. We get the exact decay widths from private communication with the authors of [31]. These are the following for $\mathrm{LQ}_3^{\mathrm{u}}$:

$$\begin{aligned}\Gamma(\mathrm{LQ}_3^{\mathrm{u}} \to t\nu) &= \frac{(m_{\mathrm{LQ}}^2 - m_t^2)^2 3\lambda^2(1-\beta)}{48\pi m_{\mathrm{LQ}}^3} \\ \Gamma(\mathrm{LQ}_3^{\mathrm{u}} \to b\tau) &= \frac{(m_{\mathrm{LQ}}^2 - m_b^2 - m_\tau^2)3\lambda^2\beta}{48\pi m_{\mathrm{LQ}}^3} \\ &\quad \times \sqrt{m_{\mathrm{LQ}}^4 + m_b^4 + m_\tau^4 - 2(m_{\mathrm{LQ}}^2 m_b^2 + m_{\mathrm{LQ}}^2 m_\tau^2 + m_b^2 m_\tau^2}),\end{aligned} \tag{2.3}$$

and for $\mathrm{LQ}_3^{\mathrm{d}}$:

$$\begin{aligned}\Gamma(\mathrm{LQ}_3^{\mathrm{d}} \to b\nu) &= \frac{(m_{\mathrm{LQ}}^2 - m_b^2)^2 3\lambda^2(1-\beta)}{48\pi m_{\mathrm{LQ}}^3} \\ \Gamma(\mathrm{LQ}_3^{\mathrm{d}} \to t\tau) &= \frac{(m_{\mathrm{LQ}}^2 - m_t^2 - m_\tau^2)3\lambda^2\beta}{48\pi m_{\mathrm{LQ}}^3} \\ &\quad \times \sqrt{m_{\mathrm{LQ}}^4 + m_t^4 + m_\tau^4 - 2(m_{\mathrm{LQ}}^2 m_t^2 + m_{\mathrm{LQ}}^2 m_\tau^2 + m_t^2 m_\tau^2}),\end{aligned} \tag{2.4}$$

where m_{LQ}, $m_t = 172$ GeV, $m_b = 4.7$ GeV and $m_\tau = 1.777$ GeV are the masses of the LQ, top quark, bottom quark and tau lepton, respectively. Figure 2.9 shows the resulting branching ratios for both models for $\beta = 0.5$. The branching ratios approach 0.5 for high leptoquark masses. These relations will be crucial for the design of the signal models in section 4.3.

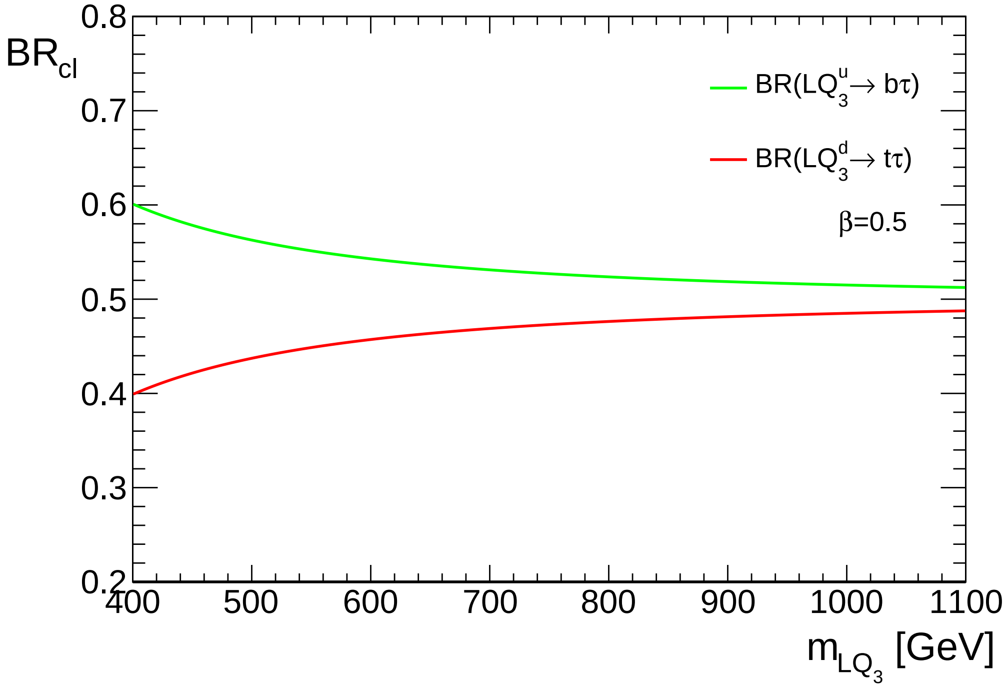

Figure 2.9: Branching ratio into charged leptons $\mathrm{BR_{cl}}$ as a function of leptoquark mass for $\mathrm{LQ_3^u}$ and $\mathrm{LQ_3^d}$ with $\beta = 0.5$.

Chapter 3

Experimental Setup

3.1 The Large Hadron Collider

The Large Hadron Collider (LHC) is the biggest and most powerful accelerator of the world. It was built underground, at a depth of about 100 m, and replaced the Large Electron Positron Collider (LEP) at CERN, where the European Organization for Nuclear Research probes the fundamental structure of particles and interactions. The LHC is used for both proton-proton (pp) collisions and heavy ion collisions.

The journey of the protons starts in a bottle of hydrogen [33]. An electric field ionizes the hydrogen atoms to make protons. These are first accelerated in the linear accelerator Linac2 and then injected into the first synchrotron, the Synchrotron Booster (BOOSTER). When they reach 1.4 GeV the protons are fed into the Proton Synchrotron (PS) where they reach 25 GeV. They are further injected into the Super Proton Synchrotron (SPS), which accelerates them to 450 GeV, when they are finally fed into the LHC as bunches in both clockwise and anticlockwise directions, such that they can collide at the center of mass energy of $\sqrt{s} = 13$ TeV. The accelerator complex is shown in figure 3.1.

The beams collide at four interaction points in the LHC, where four main experiments record the collisions. The Large Hadron Collider beauty (LHCb) focuses mainly on physics of hadrons containing b-quarks. A Large Ion Collider Experiment (ALICE) explores physics of the heavy ion collisions. The Compact Muon Solenoid (CMS) and A Toroidal LHC ApparatuS (ATLAS) are the biggest experiments. They are multi-purpose detectors and both search for new physics and measure parameters of the SM. Three smaller experiments (TOTEM, LHCf and MoEDAL), also use the LHC.

The big size of the LHC (26.7 km) allows for energetic collisions. A higher curvature would lead to more energy loss due to synchrotron radiation. The LHC ring is made up of eight arcs and eight straight sections. Superconducting magnets create high magnetic fields in order to circulate the protons around the arcs. Quadrupole and sextupole magnets focus the beams in the straight sections.

The most important parameter of the LHC, besides the center of mass energy, is the luminosity L, from which we can predict the number of events of a given process, if we know with which probability the event occurs. The number of events is given by

$$N = \sigma \int L \mathrm{d}t,$$

where σ has the dimension of an area and is a measure of the probability of the event to happen. It is usually measured in barn. $\int Ldt$ is the *integrated* luminosity, where the integration is over time. The *instantaneous* luminosity L is given by

$$L = f\frac{n_b N_b^2}{4\pi\sigma_x\sigma_y}F,$$

where n_b is the number of bunches in the proton beams, N_b the number of protons per bunch, f the revolution frequency of the bunches, σ_x and σ_y represent the dimensions of the bunches in the directions perpendicular to the beam and F corrects for the fact that the beams are not exactly perpendicular to each other [33].

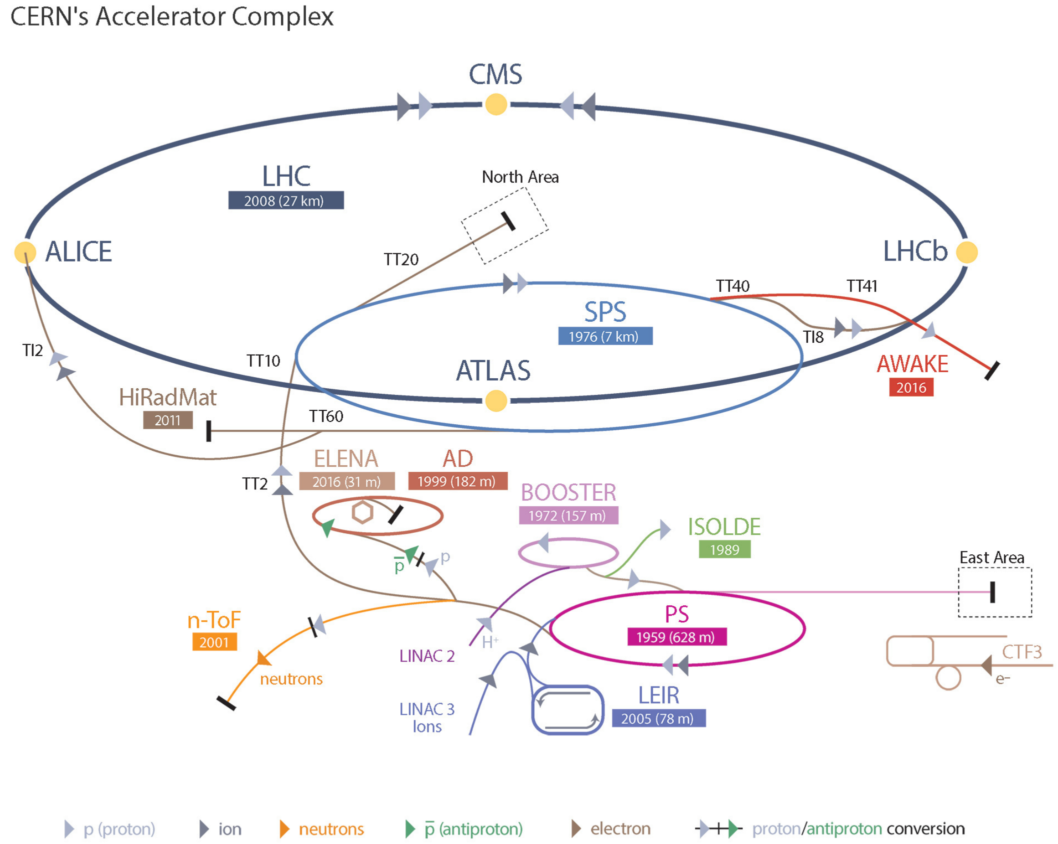

Figure 3.1: Accelerator complex at CERN [34], with the linear accelerator Linac2, the Synchrotron Booster BOOSTER, the Proton Synchrotron PS, the Super Proton Synchrotron (SPS) and the Large Hadron Collider (LHC) with its four main experiments.

3.2 The ATLAS Detector

The ATLAS detector is a 44 m long cylinder with a radius of 13 m and weighs about 7000 tonnes. BSM models usually predict new particles that either have very short lifetimes or are not directly detectable, because they only interact weakly. Therefore, ATLAS can only detect the decay products emerging from the process that we are interested in. (Meta-)stable and detectable particles may be electrons, muons, photons or hadrons. The main purpose of the detector is to measure the energy and the momentum of these decay products as well as to resolve the interaction vertices. It also has to cover as much solid angle around the interaction point as possible, in order not to miss any detectable particles. This is important because a lot of BSM models predict particles that would leave the detector undetected, like neutralinos. By covering almost the full 4π solid angle, we can measure the missing energy (in the transverse plane, for reasons we will describe in the next section).

Momentum measurements, as well as the measurement of the particle's charge, are possible with the help of a magnetic field, in which charged particles follow curved paths. By tracking the path of the particles, we can measure the radius of the curvature R and calculate the momentum p of the particle with the relation $p = eBR$, where B is the strength of the magnetic field and e the electric charge of the particle [35]. Energy measurements are performed by calorimeters. In these, particles initiate showers of decays by interacting with an active material, such that the energy of the particle is transferred, partially of fully, to the detector. There are hadronic calorimeters (HCals), which focus on the detection of hadrons, and electromagnetic calorimeters (EMCals), which focus on the detection of charged particles. Since the calorimeters absorb particles, it only makes sense to measure the momentum before we measure the energy. Therefore, the inner part of the detector, which is closest to the interaction point, is responsible for tracking charged particles and is surrounded by a magnet which creates the magnetic field. The magnet is in turn surrounded by the calorimeters. Although muons are charged, they barely interact with any of the calorimeters, due to their mass. In order to identify them and to further measure their momenta, the calorimeters are surrounded by a second magnet which creates a magnetic field in the outermost and biggest part of the detector, the muon chambers. The components of the detector are laid out as concentric cylinders around the interaction point in the so-called barrel regions and as disks to cover the top and bottom of the cylinders in the so-called end-cap regions. Figure 3.2 illustrates the layout of the ATLAS detector and shows the different components. Before describing the components in more detail, we have to introduce the coordinate systems of the detector.

3.2.1 ATLAS coordinate systems

The center of the detector and the average interaction point is the origin. The right-handed cartesian coordinate system (x, y, z) is defined such that the z-axis is parallel to the beam axis, the x-axis points towards the center of the LHC ring and the y-axis points upwards towards the Earth's surface. The cylindrical coordinates (ϕ, θ, z) use the same z-axis. ϕ is measured in the plane transverse to z, with its origin in the x-axis and θ measures the angle relative to the z-axis. The angle θ is usually expressed as pseudorapidity $\eta = \ln \tan \frac{\theta}{2}$, such that $\eta = 0$ in the transverse plane and $|\eta| = \infty$ along z.

3.2.2 Detector components

The description of the detector components is based on [36, 37].

- **Inner detector** The magnetic field of 2 T in the inner detector (ID) is created by a surrounding superconducting solenoid magnet. Tracking is performed by several different trackers. In order to resolve interaction vertices, the tracker closest to the interaction point has the highest position resolution. It is a silicon pixel detector of 80 million pixels. It is surrounded by another precision tracker, a silicon microstrip tracker (semiconductor tracker). Both precision trackers cover $|\eta| < 2.5$, which is the region of the detector devoted to precision physics. Finally, the outermost part of the inner detector is a transition radiation tracker made of straw tubes. It covers $|\eta| < 2.0$.

- **Calorimeters** The calorimeters are sampling calorimeters, which means that an active layer inducing the showers is alternated by a material used to measure the energy deposit. They cover the region of $|\eta| < 4.9$. The η region which is also covered by the ID has a fine granularity, such that the energy can be measured with high precision for particles for which we already measured the momenta. For higher values of η, we are content with lower precision, which is enough for jet reconstruction. The EMCals in the barrel region use liquid argon (LAr) as active material and lead as absorber. They are the innermost part of the calorimeter system and cover $|\eta| < 3.2$. The HCals are tile calorimeters in the barrel region and LAr detectors in the end-caps. The tile calorimeter is placed directly outside the EMCals in the barrel region. It uses scintillating tiles as active material and steel as absorber. The LAr HCal in the end-cap region uses copper as absorber. It covers up to $|\eta| = 3.2$. Finally, the region $3.1 < |\eta| < 4.9$ is covered by the LAr forward calorimeter, which is both an EMCal and a HCal. The layer closest to the interaction vertex uses copper as absorber, optimized for electromagnetic showers and the outer layers use tungsten mainly measure hadronic interactions.

- **Muon chambers** The 4000 muon chambers are embedded in the magnetic field created by the large superconducting toroid magnets. For the triggering of events and coordinate measurements, the muon system uses thin-gap chambers in the end-caps and resistive plate chambers in the barrel region. Monitored drift tubes, both in the barrel and end-cap regions, measure the curves of tracks. The curve of tracks is also measured by cathode strip chambers in the end-cap regions. The muon system covers $|\eta| < 2.7$.

3.3 Data and Monte-Carlo simulation

In high energy *pp* collisions, an event starts with the interaction of partons, which are the constituents of the protons. They can be valence quarks, sea quarks or gluons. How much momentum is transferred from the protons to the hard process and which parton will be interacting is unknown, but the probability that a specific parton carries away a certain amount of momentum is given by the parton distribution function (PDF), which can be determined experimentally. Since we do not know how much energy is transferred to the hard process, we do not have access to the total energy balance of an event. But we would like to know how much energy is missing in an event, because a lot of BSM models predict missing energy. What we do know is that the total momentum in the plane perpendicular to the z-axis is zero. This gives access to the missing transverse energy $E_{\mathrm{T}}^{\mathrm{miss}}$.

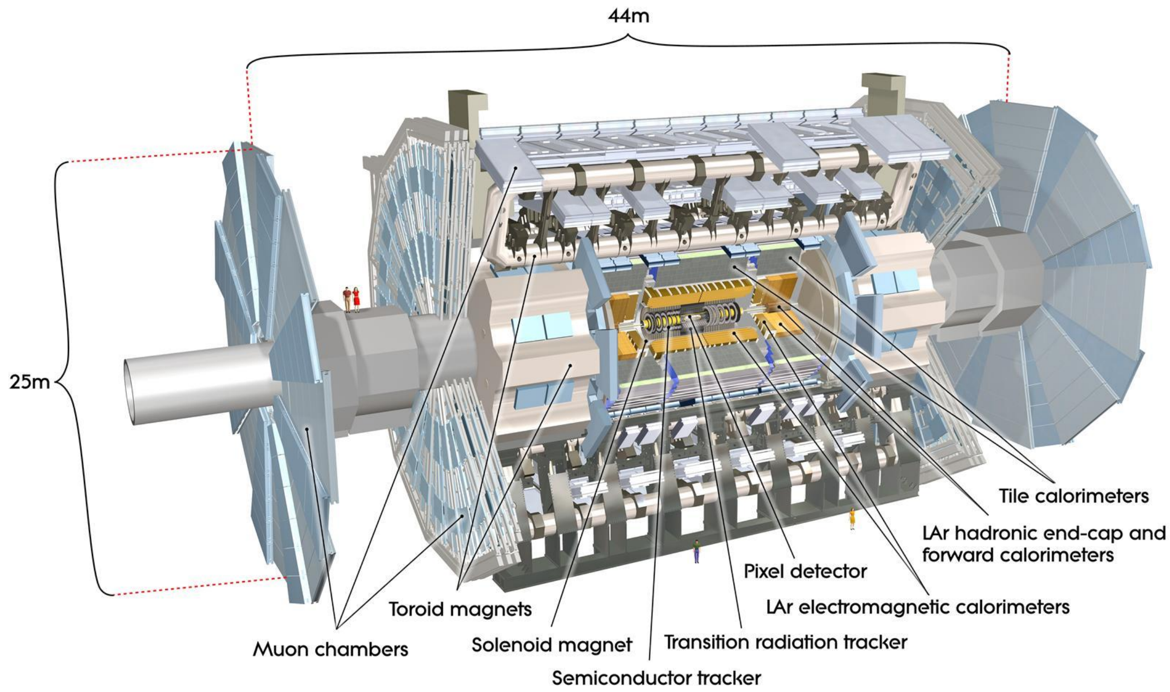

Figure 3.2: Illustration of the ATLAS detector [36]. The pixel detector and the semiconductor and transition radiation trackers are part of the inner detector. They are surrounded by the Solenoid magnet, which generates the magnetic field in the ID. It is enclosed by the calorimeter system composed of the Tile calorimeters, the liquid argon (LAr) hadronic end-cap and forward calorimeters and the LAr electromagnetic calorimeters. The calorimeters are surrounded by the toroid magnets, which generate the magnetic field in the muon chambers, the outermost part of the detector. If we look closely, we can see human beings as a reference for the size.

The hard process comes with initial and final state radiation. Once the hard process took place, partons undergo a showering process and the parton showers hadronize to form jets. These jets, which are collections of hadrons propagating in proximity to each other, will then interact with the detector, along with other (meta-)stable particles like electrons, muons or photons. Usually, a collision does not occur alone. In the same bunch crossing, many different protons collide with each other. This phenomenon is called pile-up [38].

3.3.1 Monte-Carlo simulation

In order to predict how many times a specific process occurs and what characterizes these events, we use Monte-Carlo (MC) simulation. We feed the MC algorithms with a PDF and theoretically predicted production cross-sections and decay widths. With this, we simulate the physics described above, from the hard process up to and including the interaction with the detector and the digitization of the detector response. Also pile-up and detector noise are added to the simulation. Once this is achieved, the simulated data is in the same format as the recorded data and the same reconstruction algorithms can be applied to both. Additionally, simulated data can also contain generator-level information about the physics before the inclusion of detector effects [36, 39]. We will use such information to study some aspects of leptoquark events.

3.3.2 Trigger system

The ATLAS detector can observe up to one billion *pp* collisions per second, but many of those events don't contain interesting physics and storing all this data would require a tremendous amount of storage. This is why the experiment needs a trigger system, which selects events based on characteristics that are judged to be interesting. These characteristics are typically the presence of particles like leptons or the presence of high $E_{\mathrm{T}}^{\mathrm{miss}}$. The trigger system has three levels. The lowest level trigger (L1), uses a subset of the information from the muon system and the calorimeters to decide if an event is kept. About 0.2% of the bunch crossings are kept by L1. On the second level (L2), events from L1 can be stored long enough to process the data and analyze it in more detail. A few percent of the events from L1 are kept by L2. The third level trigger (L3) makes a detailed analysis of the event with the complete detector information and uses partially the same (but often simplified versions of the) reconstruction algorithms as the ones used offline. About 200 events per second pass L3 and are stored long-term.

3.4 Particle reconstruction

In order to analyze an event, we want to identify what particles were present and we want to know their energy and momentum. But first, the detector response needs to be interpreted as detector objects, like tracks in the ID or muon chambers and energy deposits in the calorimeters. Then, we make assumptions about the particles involved. Since masses of particles are unique, one way to identify them would be to calculate their mass m with the relation $m^2 = p^2$, where p is the four-vector of energy and momentum. Unfortunately, the energy and momentum resolutions of the detector are not sufficient to distinguish particles with this method. But since different particles interact differently with the various detector components, their presence in certain components can also be used for identification. A track in the muon chamber, for example, has a high chance of being caused by a muon, since all other particles would either be absorbed in a calorimeter or leave the detector without any interaction. Figure 3.3 illustrates how particles typically interact with the components of ATLAS. The presence of secondary vertices is another important piece of information for particle identification, since it indicates the presence of a particle with a noticeable lifetime, like B-hadrons. It should be noted that the identification is never certain. We can only estimate how likely it is that a particle produces the observed detector response. If the detector response is very typical for a certain particle, the reconstructed particle is said to fulfill tight quality requirements. Using loose quality requirements means that particle misidentification is more probable. On the other hand, the reconstruction efficiency is higher for loose requirements. So we should not use tight requirements if we want to be sure not to miss a particle. In the following we will briefly describe the methods used to identify the particles relevant for our analysis.

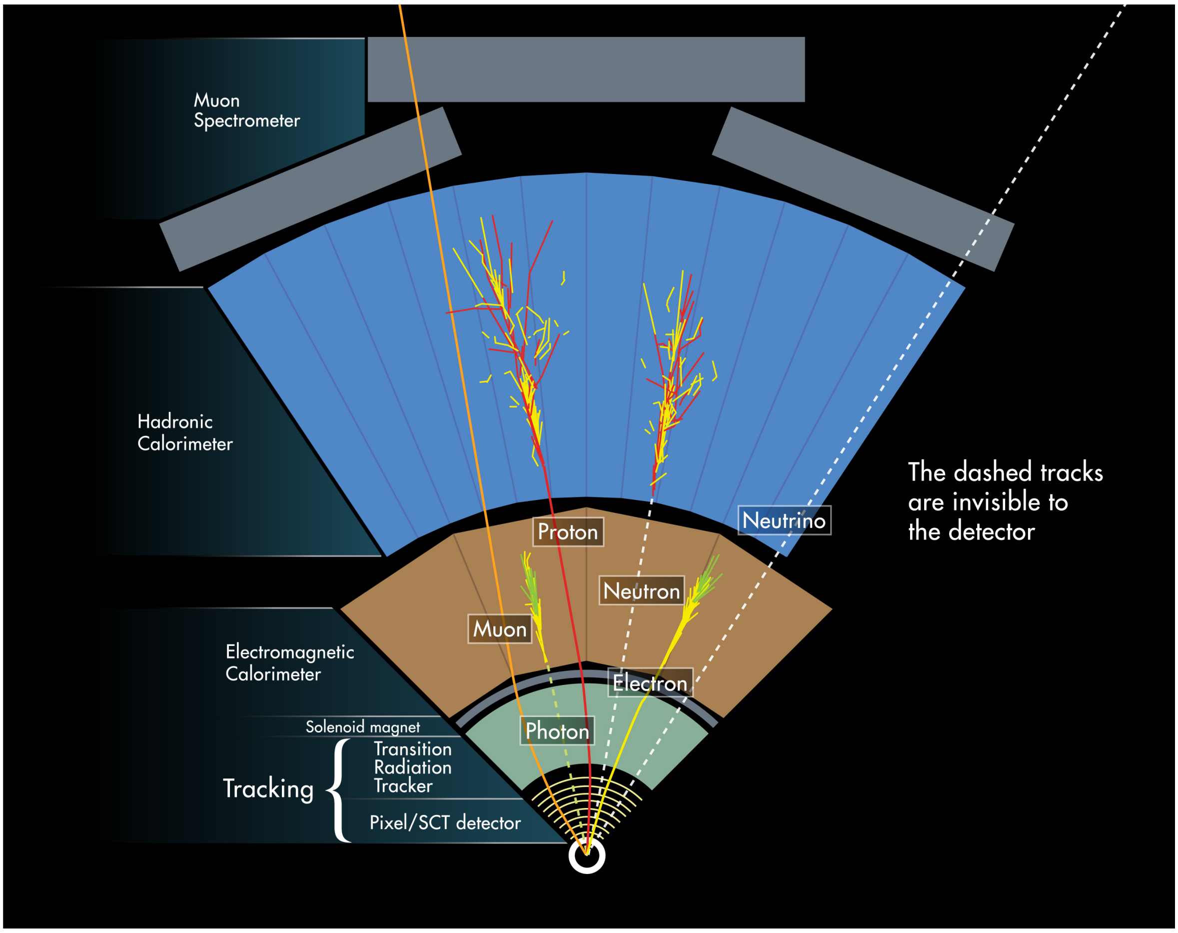

Figure 3.3: Segment of a section of the ATLAS detector illustrating how particles typically interact with the detector components [40]. Full lines indicate that the particle interacts with the detector component. Dashed lines indicate that the particle is invisible to the detector component. Only charged particles interact with the ID (tracking). Photons and electrons undergo showering in the EMCal. Charged hadrons and muons interact with the EMCal but do not undergo showering. Hadrons undergo showering in the HCal. Particles that only interact weakly, like neutrinos, do not interact with any component of the detector.

- **Electrons** Information from both the ID and the EMCal is used to reconstruct electrons. First, clusters of energy deposits in the EMCal are built to identify the presence of a charged particle and estimate the energy deposit. Then, the track pattern reconstruction is performed, using a pion hypothesis first. If the track reconstruction fails for a pion, an electron hypothesis is used instead. If a track is reconstructed successfully with an electron hypothesis and if it matches an energy deposit in the EMcal, a global likelihood based test is perfomed in order to identify it as an electron [41]. In this work, we use a tight quality requirement for the selection of electrons and a loose quality requirement for vetos.

- **Muons** Muons barely interact with the calorimeters. Therefore, mainly the muon spectrometer (MS) is used to identify them. There are three ways to identify muons in the ATLAS detector. The *standalone* reconstruction uses only information from the MS, in which it searches for patterns among hits. If patterns resemble a track, the track is extrapolated to the interaction vertex. The *combined* reconstruction, requires tracks from the MS to match tracks of the ID. The tracks from the MS and the ID are combined in order to benefit from their complementarity momentum sensitivities. Finally, identification *tagging* can be performed by tagging ID tracks with MS or calorimeter measurements. It can recover muons of low energy or in areas with limited MS coverage [42]. In this work, we require medium quality for both the selection of muons and for vetos.

- **Jets** Jets are collections of hadrons originating from the same point and propagating close to each other, such that the set of particle paths draw the shape of a cone. The hadrons create clusters of energy deposits in the calorimeters. Jet reconstruction is based on the fact that these deposits are close to each-other. The anti-k_t jet clustering algorithm [43] is used, which takes the clusters and a distance parameter (opening angle of the cone) as input. A jet-vertex-tagger (JVT) is used to reject jets originating from pile-up. Finally, the energy is calibrated using Monte-Carlo simulation and test beams. The calibration also takes into account additional energy deposits originating from pile-up and the four-momentum of the jet is chosen such that it originates from the primary vertex [44].

- ***b*-jets** Hadrons containing b-quarks have relatively long lifetimes. If such a B-hadron is produced in the hard process, a secondary vertex is formed, which can be resolved by the high precision pixel tracker of the ID. A boosted decision tree (BDT) is used to identify the jets emerging from the decay of a B-hadron. It uses information on vertices and the characteristics of the jets as input [45]. In this work, we use the MV2c10 algorithm at the 77% efficiency working point for the selection of b-jets.

- **Taus** A tau lepton has a relatively short lifetime and is therefore not directly detected by ATLAS. If it decays leptonically, the resulting light lepton is reconstructed. If it decays hadronically, we can reconstruct it from the properties of the resulting jets. Hadronically decaying tau leptons (τ_{had}) usually decay into one or three charged hadrons, such that there are either one or three tracks present in the ID. QCD jets are the main background for tau identification, but the QCD jets are usually distributed in wider angles than the jets from a τ_{had}. BDTs try to identify the τ_{had} using this information and several other input variables [46]. τ_{had} are one of the most difficult objects to identify and the reconstruction efficiencies are typically very low compared to other particles. In this work, we require medium quality τ_{had}.

3.5 Statistical Analysis

In order to find new physics, we look for what characterizes events predicted by the alternative model, that are not present in the SM. For example, a lot of BSM models predict events with high $E_{\text{T}}^{\text{miss}}$. Unfortunately, for most BSM models, there are plenty of SM processes that can yield exactly the same signatures. Usually, no variable can be found that completely discriminates the new physics events from the SM events. Therefore, we can never tell if a specific event is a SM background or if it is a signal event emerging from new physics. Instead, we can measure *how many* events with specific characteristics occur and with statistical inference, we can quantify how likely this amount can be explained by a specific hypothesis. We consider two hypotheses. The *background-only* hypothesis H_b states that there is no new physics beyond the standard model. The *signal-plus-background* hypothesis H_{s+b} states that besides the known processes of the standard model, there are events only explained by new physics. We call these new physics events signal events. Signal regions (SRs) are chosen such that the ratio of signal over background events is as big as possible, or more precisely, such that we maximize the significance, which we will define below. We introduce the signal strength paramater μ, such that the total expected number of events is $n = \mu s + b$, where s is the expectation value of the number of signal events and b is the expectation value of the number of background events. $\mu = 0$ for H_b and $\mu = 1$ for H_{s+b}.

We will introduce basic concepts in the simplified situation where the background is exactly known and describe the test statistic used in this work and the way we handle auxiliary measurements and uncertainties later.

3.5.1 Concepts

The probability to observe a given amount of events N, for a total number of expected events n is given by the Poisson distribution,

$$\mathcal{P}(N, n) = \frac{n^N}{N!} e^{-n}. \tag{3.1}$$

We define the likelihood L for a given hypothesis H as the probability to observe the N_o number of events that we measured, under the condition that H is true:

$$L(N_o|H) = P(N_o|H).$$

We use the p-value p to decide whether we reject a hypothesis or not. It is defined as the probability to observe what we have measured or to observe something less compatible with a given hypothesis. If we have observed more events than we expected from H_b and want to claim a discovery, we have to reject H_b. I that case, we can use

$$p_b = \sum_{N=N_o}^{\infty} \mathcal{P}(N, b),$$

because observing any higher number of events than N_o is less compatible with H_b. If we observed less events than expected from H_{s+b} and want to reject this alternative hypothesis, we can use

$$p_{s+b} = \sum_{N=0}^{N_o} \mathcal{P}(N, s + b),$$

The p-values can be turned into a number of Gauss standard deviations, which we call the significance Z and is given by

$$Z = \phi^{-1}(1 - p),$$

where ϕ^{-1} is the inverse cumulative distribution function of a standard Gauss distribution.

We define a significance level α, such that we exclude a hypothesis if $p < \alpha$. We use the confidence level CL $= 1 - p$ to present the result and use $\alpha = 0.05$ as a threshold for the exclusion of an alternative hypothesis, which is a common choice in particle physics[1]. If we say we exclude H at 95% CL ($\alpha = 0.05$), it means that if H is in reality true and we repeat the experiment, 5% of the time we will observe a result that is also at least as incompatible with H.

[1] In order to claim an evidence (discovery) of a new particle, $p < 0.003$ ($p < 0.0000003$) is required, which corresponds to 3σ (5σ) significance.

Depending on the observation, using CL_{s+b} can potentially exclude H_{s+b}, even though the experiment has a low sensitivity to the signal. Indeed, if both hypotheses predict about the same number of events, and we observe an unlikely downward fluctuation, then p_{s+b} will be low, but the result is almost just as incompatible with H_b. In order to avoid this, we use

$$\mathrm{CL}_s = \frac{p_{s+b}}{1-p_b}$$

instead [47]. This tells us how unlikely the observation is assuming H_{s+b}, compared to how unlikely it is assuming H_b. The CL_s method is more conservative than CL_{s+b} and although it is controversial amongst statisticians, its usage is common in particle physics.

This procedure allows to calculate *observed* limits. When calculating *expected* limits, we do not use the measurement N_o, but replace it by the expectation of the hypothesis that we do not intend to exclude, i.e., $s+b$ for p_b and b for p_{s+b}.

Another tool that we will use is the upper-limit scan for the exclusion of H_{s+b}. The principle is to scale signal strength μ to the value for which we would exclude H_{s+b} at significance level α. The result is the ratio of the signal cross-section that we can exclude over the expected signal cross-section.

3.5.2 Profile likelihood ratio

Until now we have assumed a single background which we described with a fixed model without uncertainty. In this work we consider several backgrounds and perform auxiliary measurements in control regions (CRs), which are designed to hold a high amount of the background events we want to measure and only few signal events, which are considered as contamination in this context. In this case, the total background expectation in the SR becomes $b = \sum \tau_i b_i$ with b_i referring to the Monte-Carlo expectations of individual background processes in the SR and τ_i being the normalization factors obtained from the auxiliary measurements. In the case where there is only one source of background and we normalize it in one CR, then $\tau = N_{\mathrm{CR}}^{\mathrm{data}}/b_{\mathrm{CR}}^{\mathrm{MC}}$, where $b_{\mathrm{CR}}^{\mathrm{MC}}$ is the Monte-Carlo expectation of the background in the CR and $N_{\mathrm{CR}}^{\mathrm{data}}$ is the number of observed events in the CR. In reality, all backgrounds, and potentially signal events, can contribute to $N_{\mathrm{CR}}^{\mathrm{data}}$ and we calculate the τ_i by maximizing the likelihood described below. We do account for signal contamination when calculating the τ_i. This has an impact on the normalization factors when the signal is absent in data, since background and signal have to "share" $N_{\mathrm{CR}}^{\mathrm{data}}$.

We also consider sources of systematic uncertainties, which affect the expectation value of the Poisson distributed number of events in the SR. All systematic uncertainties and normalization factors are summarized in the vector of nuisance parameters $\boldsymbol{\theta}$. Each nuisance parameter θ_j is modeled with an additional probability distribution function $C_j(\theta_j^0, \theta_j)$, where θ_j^0 is the mean value. We also consider using more than one SR and we summarize the measurements in the SRs with the vector of observed number of events $\boldsymbol{N_o}$. We consider the following likelihood:

$$L(\mu, \boldsymbol{\theta}) = L(\boldsymbol{N_o}|\mu, \boldsymbol{\theta}) = \prod_{k \in \mathrm{SRs,CRs}} \mathcal{P}(N_o^k, n^k(\boldsymbol{\theta}, \mu)) \prod_j C_j(\theta_j^0, \theta_j), \tag{3.2}$$

where the signal strength μ denominates the hypothesis. This is a product of poisson terms for each observation in a SR or CR N_o^k. The expected number of events is now a function of the nuisance parameters and the signal strength. This product is further multiplied by the terms $C_j(\theta_j^0, \theta_j)$, which constrain the nuisance parameters. Previously, we used a fixed model describing our background. Now we fit it to data by maximizing the likelihood 3.2. We also implicitly used the number of events in the signal region N as a test statistic. A test statistic can be any function of the measurement that is a single number and it should be chosen such that it distinguishes behaviors of the different hypothesis that we want to test. The previous choice did have this distinguishing power, but the Neyman-Pearson lemma states that the most powerful test is given by the likelihood ratio test [48]. We will use the log-likelihood ratio

$$\lambda(\mu) = -2\ln\frac{L(\mu, \hat{\hat{\boldsymbol{\theta}}})}{L(\hat{\mu}, \hat{\boldsymbol{\theta}})} \tag{3.3}$$

as a test statistic, where $\hat{\hat{\boldsymbol{\theta}}}$ is the set of nuisance parameters obtained by maximizing the likelihood for a fixed μ and $\hat{\boldsymbol{\theta}}$ and $\hat{\mu}$ are the nuisance parameters and the signal strength obtained by maximizing the likelihood with floating μ[2]. Simply speaking, this tells us how likely a measurement is, assuming a specific choice of μ (choice of hypothesis), compared to the likelihood of the most likely choice of μ. Now, we calculate the p-values with

$$p(\mu) = \int_{\lambda^o(\mu)}^{\infty} f(\lambda(\mu))d\lambda, \tag{3.4}$$

where f is the probability distribution function for $\lambda(\mu)$ at a given μ and where the integration goes from the observed value of the log-likelihood ratio $\lambda^0(\mu)$ to infinity. Determining the exact function f requires the computation of so-called toy experiments, which is very time consuming and computing intensive. We calculate it using the asymptotic formula [49] instead.

Now, when we calculate CL_b, we use $\lambda(\mu = 0)$ and for CL_{s+b}, we use $\lambda(\mu = 1)$. It should be noted that p_b and therefore CL_b are now not independent of the alternative hypothesis, since in the denominator of the log-likelihood ratio defined by equation 3.3, we maximize the likelihood with a free signal strength μ. μ is only fixed at 0 in the numerator.

The likelihood 3.2 is also used for the *background-only* fit, but without considering yields in the SRs and assuming that all data in the CRs come from background processes. It is not used for statistical inference, but to calculate the values of nuisance parameters under the H_b hypothesis. Especially the obtained normalization factors are of interest. Indeed, these normalization factors are used to validate that the background normalization can be extrapolated into the SRs. This is done by inspecting the yields in validation regions (VRs), which lye kinematically in between the CRs and SRs.

The statistical analysis is performed with the framework HistFitter [50].

[2]We use the same prescription as in [49] for $\hat{\mu} < 0$ or $\hat{\mu} > \mu$.

Chapter 4

Reinterpretation

4.1 Introduction

A physics analysis in the ATLAS experiment is a long-lasting effort usually performed by a team of physicists. A sizable part of the work consists in understanding the SM background, evaluating the uncertainties, setting up the analysis framework and debugging. Interpreting the result for a given model comes at the end and is, in terms of workload, a much smaller effort. Although an analysis is usually built to target a specific BSM model, the considered phase-space is generally also sensitive to other BSM processes. Hence, it makes sense, before starting a new analysis optimized for LQ_3 models, to see if in the pool of existing analyses, we find one that has good acceptance to our signal models.

The final states of third generation leptoquarks contain tau leptons, b-quarks and $E_{\mathrm{T}}^{\mathrm{miss}}$. One analysis which targets such final states is the search for top squarks pair production decaying to tau sleptons [1], for which we will use the shorthand stop-stau. The reinterpretation of this analysis in terms of LQ_3 is the topic of this thesis. Other possible choices could be searches for pair-produced top or bottom squarks without intermediate tau sleptons or a search for Higgs bosons in the $bb\tau\tau$ channel. Reinterpretations in terms of third generation leptoquarks are indeed being performed for such searches. The sensitivities of these analyses are high for values of β close to 0 or 1, respectively, but drop off quite quickly for intermediate values of β. The stop-stau search, as we will see later, is most sensitive to the intermediate values of β.

The outline of this chapter is as follows: An overview of the stop-stau analysis is given in section 4.2. In section 4.3, the LQ_3 signal models are described. In section 4.4, the LQ_3 signal models are compared to the original benchmark model of the stop-stau analysis. Finally, the results are presented in section 4.5.

4.2 The stop-stau analysis

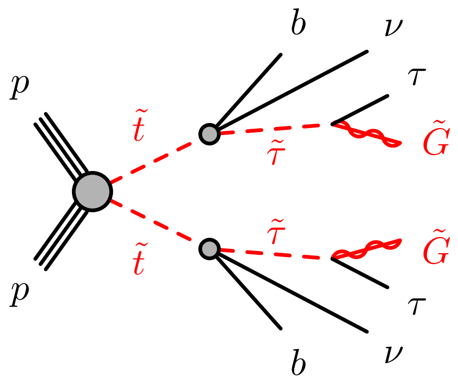

Figure 4.1: Diagram of the stop-stau signal model.

The benchmark scenario targeted by the analysis is schematically depicted in figure 4.1. This process considers pair produced top squarks, in which both top squarks decay via a 3-body decay into tau slepton, a b-quark and neutrino. Each tau slepton further decays to a tau lepton and a gravitino. In this simplified model, motivated by gauge mediated SUSY breaking and natural gauge mediation, the only supersymmetric particles considered are the lightest top squark $\tilde{t}_1$, the lightest tau slepton $\tilde{\tau}_1$ and the gravitino $\tilde{G}$. All other sparticles are assumed to be heavy enough to not play any role in the decay chain. The gravitino is assumed to be the LSP and to leave the detector without interaction. We expect a signature with high $E_{\mathrm{T}}^{\mathrm{miss}}$, coming from the gravitinos and neutrinos. Furthermore, we expect jets originating from B-hadrons. From the decay of the tau leptons, we expect either light leptons or a τ_{had}. We also expect the two tau leptons to be of opposite sign (OS).

The analysis considers two decay-channels: the lep-had channel, which targets events with one leptonically and one hadronically decaying tau lepton, and the had-had channel, which targets events where both taus decay hadronically. The lep-lep channel, which would target events where both tau leptons decay leptonically, is not considered. In appendix A.1, we show that this channel would barely contribute to the final result, the main reason being that the branching ratio of the decay of two tau leptons in two light leptons is only about 12%.

After overlap removal[1] and event-cleaning[2], a preselection of events is made for each channel, which is mainly defined by requirements on the multiplicities of reconstructed objects. This ensures that the variables needed for the definition of the signal and control regions can be defined, and also gets rid of a large number of background events. In the lep-had channel, as one light lepton (electron or muon) ℓ is expected from the decay of the tau lepton, events selected by either a single electron or a single muon trigger are used. The preselection for this channel requires exactly one light lepton with transverse momentum $p_{\mathrm{T}} > 25$ GeV and $\eta < 2.47$ if it is an electron and $\eta < 2.7$ if it is a muon, one τ_{had} with $p_{\mathrm{T}} > 20$ GeV and $\eta < 2.47$ and at least two jets with $p_{\mathrm{T}} > 26$ GeV. In the had-had channel, events selected by a $E_{\mathrm{T}}^{\mathrm{miss}}$ or a ditau trigger are used. Here, exactly two τ_{had} with $p_{\mathrm{T}} > 20$ GeV and $\eta < 2.47$ and at least two jets with $p_{\mathrm{T}} > 20$ GeV are required in the preselection and events with additional light leptons are rejected. Additional requirements are made on the transverse

[1] Since the reconstruction algorithms run independently from each other, the same physical object can be recorded as several reconstructed objects. In order to count each physical object only once, we remove some of the reconstructed objects if there are several close to each other.

[2] Event cleaning ensures that we select only events for which the detector was fully functional, that a primary vertex was found and that the event has a low probability to contain unwanted objects such as cosmic muons or jets from instrumental effects.

momentum of the light lepton, the leading $\tau_{\rm had}$ or on $E_{\rm T}^{\rm miss}$, depending on which trigger has fired. This ensures that the triggers are only used in the plateau regions, where the efficiency is constant and maximal. Requirements are also made for the quality, the isolation and the spacial origin of the selected objects.[3] The preselection requirements are summarized in table 4.1.

	lep-had	had-had
Triggers Trigger requirements	single electron or muon cuts on lepton $p_{\rm T}$	$E_{\rm T}^{\rm miss}$ or ditau cut on $E_{\rm T}^{\rm miss}$or $p_{\rm T}(\tau_{1,2})$ and $p_{\rm T}(j_1)$, depending on which trigger fired
# τ	1	2
# ℓ	1	0
# jets	≥ 2 $p_{\rm T}(j_2) > 26$ GeV	≥ 2

Table 4.1: Requirements for events to pass the lep-had or had-had preselection. $\tau_{1,2}$ are the leading and subleading $\tau_{\rm had}$ and $j_{1,2}$ are the leading and subleading jets.

For each channel, one signal region is defined, which we combine statistically with the method described in section 3.5. Before giving more details about the analysis strategy, we describe the variables used to define the signal and control regions.

In the following if a variable is computed from the four-momenta of two particles ρ_1 and ρ_2, the four momenta refer to the ones of the selected leptons of the respective channel. I.e., $(\rho_1, \rho_2) = (\ell, \tau)$ for the lep-had channel and (τ_1,τ_2) for the had-had channel, where τ_1 (τ_2) refers to the leading (subleading) $\tau_{\rm had}$.

Missing transverse energy The missing transverse energy $E_{\rm T}^{\rm miss}$ is the magnitude of the missing transverse momentum, which is calculated as the negative sum of the transverse momenta of all reconstructed objects in the event and the energy of tracks that were not matched to any reconstructed object.

Invariant mass The invariant mass of two particles is defined as

$$m(\rho_1, \rho_2)^2 = (E_{\rho_1} + E_{\rho_2})^2 - (\mathbf{p}_{\boldsymbol{\rho_1}} + \mathbf{p}_{\boldsymbol{\rho_2}})^{\mathbf{2}},$$

which is equal to the mass of the mother particle if ρ_1 and ρ_2 are its decay products. This variable is very useful to identify events containing a specific mother particle that decays into visible objects, for example $Z \to \ell\ell$.

Transverse mass As mentioned in section 3.4, the missing energy in the axis of the beamline is unknown. As a consequence, if a particle, like a W boson, decays partly into undetectable objects like neutrinos, we cannot calculate its invariant mass. Instead, we can calculate its transverse mass

$$m_{\rm T}^2 = (E_{\rm T}(\rho) + E_{\rm T}^{\rm miss})^2 - (\mathbf{p}_{\rm T}(\rho) + \mathbf{E}_{\rm T}^{\rm miss})^2,$$

which is the invariant mass in the transverse plane, i.e. calculated with the transverse components of energy and momentum. The transverse mass is constructed such that it is bound by the mass of the mother particle $m_{\rm T} \leqslant m$, but in practice the invisible particle is rarely the only source of $E_{\rm T}^{\rm miss}$, which smears out the distribution of $m_{\rm T}$. It has good discrimination power for events containing W bosons.

[3] Requirements are looser on objects by which events are vetoed.

Stransverse mass The stransverse mass m_{T2} can be used for events in which two particles of the same kind decay semi-invisibly, like in $WW \to \ell\ell\nu\nu$. In this case, estimating the mass becomes more difficult, as we only have access to the total $E_{\mathrm{T}}^{\mathrm{miss}}$ and do not know the individual sources. But if we try all possible ways to distribute $E_{\mathrm{T}}^{\mathrm{miss}}$ such that $\mathbf{E}_{\mathrm{T}}^{\mathrm{miss}} = \mathbf{E}_{\mathrm{T1}}^{\mathrm{miss}} + \mathbf{E}_{\mathrm{T2}}^{\mathrm{miss}}$ and calculate m_{T} for both particles using $\mathbf{E}_{\mathrm{T1}}^{\mathrm{miss}}$ and $\mathbf{E}_{\mathrm{T2}}^{\mathrm{miss}}$ and choose the m_{T} which is bigger, then the smallest value we get is still bound by the mass value of the mother particles:

$$m_{\mathrm{T2}}^2(\rho_1, \rho_2) = \min_{\mathbf{E}_{\mathrm{T}}^{\mathrm{miss}} = \mathbf{E}_{\mathrm{T1}}^{\mathrm{miss}} + \mathbf{E}_{\mathrm{T2}}^{\mathrm{miss}}} [\max(m_{\mathrm{T}}^2(\rho_1, \mathbf{E}_{\mathrm{T1}}^{\mathrm{miss}}), m_{\mathrm{T}}^2(\rho_2, \mathbf{E}_{\mathrm{T2}}^{\mathrm{miss}}))] \leqslant m^2.$$

Again, the m_{T2} distribution gets smeared out by additional sources of $E_{\mathrm{T}}^{\mathrm{miss}}$, but as we will see later, it is a powerful variable to discriminate the stop-stau signals from events where two W bosons are involved, especially if the tau slepton has a much higher mass than the W boson.

Effective mass The effective mass is defined as

$$m_{\mathrm{eff}} = E_{\mathrm{T}}^{\mathrm{miss}} + p_{\mathrm{T}}(j_1) + p_{\mathrm{T}}(j_2) + p_{\mathrm{T}}(\rho_1) + p_{\mathrm{T}}(\rho_2),$$

where j_1 and j_2 refer to the leading and subleading jets. This variable generally has high values for events in which heavy particles decay, such that the decay products have high transverse momenta.

4.2.1 Event selection and background estimation

The most important SM background is top pair production ($t\bar{t}$), that contributes in two ways: Either the W boson from the top decay really decays into a tau lepton and is successfully reconstructed, or it decays hadronically or into a light lepton, and the resulting jet is falsely reconstructed as originating from a tau lepton.[4] We call the first contribution $t\bar{t}$ *real* and the second $t\bar{t}$ *fake*. Sub-dominant contributions come from diboson production, where jets are often falsely identified as originating from a B-hadron, and top pair production in association with a vector boson ($t\bar{t} + V$).

In total five control regions are used, with three of them dedicated to constrain $t\bar{t}$ modeling. For events in the had-had channel, one control region is designed for the contributions from $t\bar{t}$ *real* and one for $t\bar{t}$ *fake*. In the lep-had channel, a region for $t\bar{t}$ *real* is also defined but a fake-factor method[5] (FFM) is used to estimate fake contributions. Diboson production and top pair production in association with a vector boson are also normalized in dedicated control regions, which are common to both channels.

The signal regions (SR LH for the lep-had channel and SR HH for the had-had channel) both require high m_{T2}, high $E_{\mathrm{T}}^{\mathrm{miss}}$, a τ_{had} with high transverse momentum and require the selected leptons to be of opposite sign. Tables 4.2 to 4.4 summarize the cuts defining the signal and control regions. Validation regions, which are kinematically in between the control and the signal regions, are also defined. These are not used to interpret the data, but to ensure that the normalization factors, calculated in the control regions, can be extrapolated to the signal regions.

[4] It is also possible that the real tau lepton is not reconstructed and that some other source fakes one.

[5] The FFM measures the proportion of events with fakes in a dedicated measurement region. The resulting fake-factor is then applied to the $t\bar{t}$ *real* count, to give an estimate of $t\bar{t}$ *fake*.

SR LH	SR HH
selected leptons have opposite charge	
# b-jets $\leqslant 1$	
$p_{\mathrm{T}}(\tau_1) > 70$ GeV	
$m_{\mathrm{T2}}(\ell,\tau) > 100$ GeV	$m_{\mathrm{T2}}(\tau,\tau) > 80$ GeV
$E_{\mathrm{T}}^{\mathrm{miss}} > 230$ GeV	$E_{\mathrm{T}}^{\mathrm{miss}} > 200$ GeV

Table 4.2: Requirements for the lep-had and had-had signal regions.

Variable	CR HH $t\bar{t}$ *real*	CR HH $t\bar{t}$ *fake*
preselection	had-had	
sign(τ,τ)	opposite sign	—
# b-jets	$\leqslant 1$	
$E_{\mathrm{T}}^{\mathrm{miss}}$	> 120 GeV	
$p_{\mathrm{T}}(\tau_1)$	> 70 GeV	
$m_{\mathrm{T2}}(\tau_1,\tau_2)$	< 30 GeV	
$m(\tau_1,\tau_2)$	> 70 GeV	
$m_{\mathrm{T}}(\tau_1)$	> 70 GeV	< 70 GeV

Variable	CR LH $t\bar{t}$ *real*
preselection	lep-had
sign(ℓ,τ)	opposite sign
# b-jets	$\leqslant 1$
$E_{\mathrm{T}}^{\mathrm{miss}}$	> 210 GeV
$p_{\mathrm{T}}(\tau)$	> 70 GeV
$m_{\mathrm{T2}}(\ell,\tau)$	< 60 GeV
$m_{\mathrm{T}}(\ell)$	> 100 GeV

Table 4.3: Requirements for the $t\bar{t}$ control regions.

4.2.2 Background-only fit and results

Tables 4.5 and 4.6 are taken from the published analysis results [1]. Table 4.5 shows the number of observed events, the background expectation from the background-only fit and the Monte-Carlo expectation of a stop-stau signal in the signal regions. The table includes statistical and systematic uncertainties. The biggest systematic uncertainty in the lep-had channel comes the fake factor method. Different components contribute to this uncertainty. The main one comes from the fact that there is a different fake composition in the FFM measurement region than in the SR. In the had-had channel, the biggest systematic uncertainty is related to tau identification. The search did not observe an excess of events and the result is in good agreement with the SM prediction.

Table 4.6 shows the normalization factors obtained from the background-only fit.

	CR $t\bar{t}+V$	CR VV
$p_{\mathrm{T}}(j_2)$	> 26 GeV	
# SFOS	$\leqslant 1$	
m_Z^{closest}	[80-100] GeV	
# b-jets	$\leqslant 2$	0
# ℓ	$\leqslant 3$	$\leqslant 2$
# $\ell + j$	$\leqslant 6$	—
$E_{\mathrm{T}}^{\mathrm{miss}}/\sqrt{H_{\mathrm{T}}}$	—	$> 15\sqrt{\mathrm{GeV}}$
$m_{\mathrm{T2}}(\ell,\ell)$	—	< 120 GeV

Table 4.4: Requirements for the common control regions for $t\bar{t}+V$ and diboson. SFOS stands for same flavor opposite sign lepton pair. The invariant mass of the SFOS closest to the mass of the Z boson is m_Z^{closest}. H_{T} is the scalar sum of the transverse momenta of the two leading jets.

	SR LH	SR HH
Observed events	3	2
Total background	2.2 ± 0.6	1.9 ± 1.0
Fake $\tau_{had} + e/\mu$	1.4 ± 0.5	—
$t\bar{t}$ *fake*	—	$0.6 \pm^{0.7}_{0.6}$
$t\bar{t}$ *real*	0.22 ± 0.12	$0.28 \pm^{0.30}_{0.28}$
$t\bar{t}+V$	0.25 ± 0.14	0.26 ± 0.12
Diboson	0.15 ± 0.11	0.28 ± 0.13
Single-top	$0.10 \pm^{0.24}_{0.10}$	0.13 ± 0.11
V+jets	0.032 ± 0.014	0.26 ± 0.09
Others	0.082 ± 0.022	0.09 ± 0.04
SS(1100,590)	3.3 ± 0.7	4.7 ± 1.2

Table 4.5: Observed number of events, background expectation from the background-only fit and Monte-Carlo expectation of the yield of a stop-stau signal with $(m_{\tilde{t}}, m_{\tilde{\tau}}) = (1100, 590)$ GeV in the signal regions. Fake $\tau_{had}+e/\mu$ are events including a fake τ_{had} and an light lepton. The uncertainties include both systematic and statistical uncertainties.

Process	Normalization factor
Diboson	$1.0\ ^{+0.6}_{-0.3}$
$t\bar{t}+V$	$1.39^{+0.23}_{-0.23}$
$t\bar{t}$ *fake*	$1.2\ ^{+0.4}_{-0.4}$
$t\bar{t}$ *real*	$0.81^{+0.20}_{-0.20}$

Table 4.6: Normalization factors obtained from the background-only fit. The normalization factor for $t\bar{t}$ events with fake tau leptons is not applied in the lep-had channel, where the FFM is used.

4.3 Leptoquark signal models

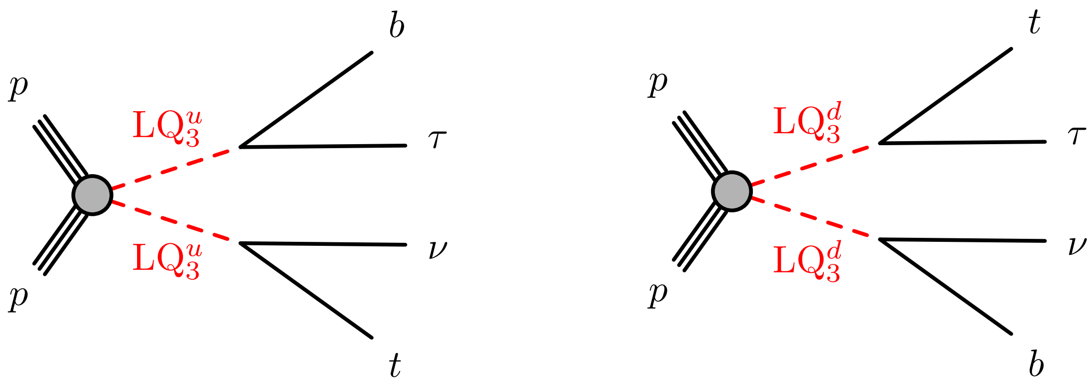

Figure 4.2: Diagrams of LQ_3^u and LQ_3^d pair production, with each LQ decaying to a different final state. The two leptoquarks decay independently either as shown in the upper or the lower branch.

We consider the two simplified models presented in section 2.3: up-type (LQ_3^u) and down-type (LQ_3^d) scalar leptoquarks of third generation. LQ_3^u can decay into either $[b,\tau]$ or $[t,\nu]$ and LQ_3^d can decay into either $[t,\tau]$ or $[b,\nu]$. The signal models consist of pair production of these, such that the possible final states for the LQ_3^u model are $[b,\tau][b,\tau]$, $[b,\tau][t,\nu]$ or $[t,\nu][t,\nu]$ and for the LQ_3^d model the possible final states are $[t,\tau][t,\tau]$, $[t,\tau][b,\nu]$ or $[b,\nu][b,\nu]$. Figure 4.2 shows the diagrams in the case of mixed final states. The decay channel of a pair of leptoquarks can be characterized using the number of charged leptons in the final state (n_{cl}), which can be 0, 1 or 2.

We fix the Yukawa coupling strength parameter λ to 0.3, which can be considered as a natural choice as it corresponds to the same strength as electromagnetic interactions. For our purpose, λ would only affect the decay widths, as we neglect lepton exchange as a production mechanism and, looking at equations 2.3 and 2.4, we realize that all widths have the same dependency on λ, such that its value does not affect the phenomenology of the events. Only very small values of λ would affect the phenomenology, since then, leptoquarks would be meta-stable. This would give rise to completely different signatures. So fixing λ at 0.3 indeed seems like a reasonable choice.

As discussed in section 2.3, the branching ratio of the decay of a LQ into a charged lepton and a quark (BR_{cl}) is determined by the parameter β of the model. In order to fully explore possible third generation leptoquark models, we have to consider a 2-dimensional grid of signals, with the LQ mass and β, or BR_{cl}, as parameters. It is not necessary to simulate the whole grids though. Indeed, as events with n_{cl}=0, 1 and 2 are all available in samples with intermediate values of β, we can vary this parameter by attributing weights to the different classes of events, such that the resulting collection of events is equivalent to what would have been produced with a different value of β. (For example, we can produce a sample with β=0 by removing all events with n_{cl}=1 and 2 from a sample produced with β=0.5 and then attributing larger weights to the remaining events in order to preserve the total production cross-section.) In order to do this, we need to know the branching ratio into charged leptons of the original sample, $\hat{BR}_{cl}$. In the original sample, the rate at which events with n_{cl}=2 occur is $\hat{BR}_{cl}{}^2$. If we want the rate to be $BR_{cl}{}^2$, then we need to assign these events a weight of $\frac{BR_{cl}^2}{\hat{BR}_{cl}{}^2}$. With a similar reasoning for other n_{cl}, we conclude that the event weights for the three classes of events ($n_{\mathrm{cl}} = 0, 1, 2$) are given by:

$$w_{\mathrm{n_{cl}}}(\mathrm{BR_{cl}}) = \left(\frac{\mathrm{BR_{cl}}}{\hat{\mathrm{BR}}_{\mathrm{cl}}}\right)^{\mathrm{n_{cl}}} \left(\frac{1-\mathrm{BR_{cl}}}{1-\hat{\mathrm{BR}}_{\mathrm{cl}}}\right)^{2-\mathrm{n_{cl}}} . \tag{4.1}$$

We consider LQ masses from 400 to 1100 GeV in steps of 100 or 50 GeV and $\mathrm{BR_{cl}}$ between 0 and 1, in steps of 0.1. The full list of samples used is given in appendix A.3, together with $\hat{\mathrm{BR}}_{\mathrm{cl}}$ and the production cross-sections, which is a calculation from [51].

To conclude this section, let's inspect the final states of both models for different $\mathrm{BR_{cl}}$, using generator-level information. Figure 4.3 shows the number of tau leptons, the number of b-jets and $E_{\mathrm{T}}^{\mathrm{miss}}$ of simulated $\mathrm{LQ_3^u}$ and $\mathrm{LQ_3^d}$ signals with $m_{\mathrm{LQ}} = 750$ GeV. Both leptonically and hadronically decaying tau leptons are counted in the distributions shown, such that, as expected, we always find at least two of them for $\mathrm{BR_{cl}}$= 2. We see that we get the highest multiplicity of tau leptons from $\mathrm{LQ_3^d}$ with $\mathrm{BR_{cl}}$= 2, where they can additionally originate from the decay of the top quark or from the resulting b-quark (although the ones from the b decay have rather low momenta). $\mathrm{LQ_3^d}$ with $\mathrm{BR_{cl}}$= 0 yields the least amount of tau leptons, as they can only originate from the decay of the b-quark. The number of b-jets is almost always 2 for all signals, since the top quark decays to Wb with a branching ratio of about 99.8%. The distribution of $E_{\mathrm{T}}^{\mathrm{miss}}$ does not seem to depend on the type of LQ, but does depend on $\mathrm{BR_{cl}}$. We get higher values when neutrinos originate directly from an LQ and lower values when neutrinos only appear from subsequent decays of tau leptons or top and bottom quarks. Finally, we observe that for all distributions shown here, $\mathrm{LQ_3^u}$ and $\mathrm{LQ_3^d}$ with $\mathrm{BR_{cl}}$= 0.5 are equivalent, as the final states are the same. Only the pairing is different, which plays a role for the variable m_{T2}, as we will see in the next section.

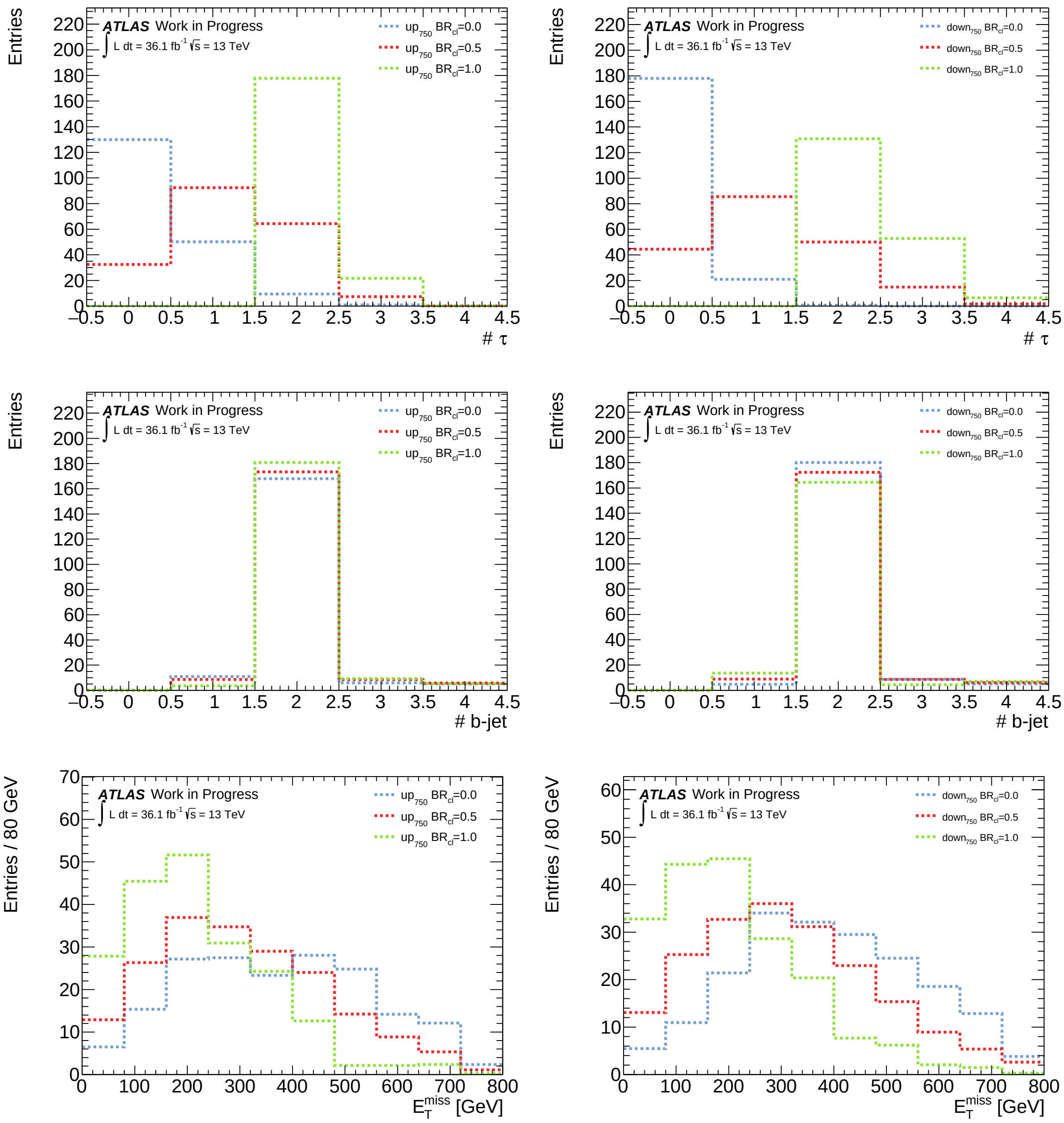

Figure 4.3: Number of tau leptons τ, number of b-jets and $E_{\mathrm{T}}^{\mathrm{miss}}$ distributions for $\mathrm{LQ}_3^{\mathrm{u}}$ (left) and $\mathrm{LQ}_3^{\mathrm{d}}$ (right) signals with a $\mathrm{BR}_{\mathrm{cl}}$ of 0, 0.5 and 1 and m_{LQ}=750 GeV, illustrating the differences in the final states.

4.4 Signal comparison

From the diagrams of $\mathrm{LQ}_3^{\mathrm{u}}$ and $\mathrm{LQ}_3^{\mathrm{d}}$ shown in figure 4.2 and from the diagram of the stop-stau signal shown in figure 4.1, we see that the final states of the models are similar. The final state of the stop-stau signal always contains 2 b-quarks, 2 tau leptons and $E_{\mathrm{T}}^{\mathrm{miss}}$. The LQ signals also always contain 2 b-quarks and have sources of $E_{\mathrm{T}}^{\mathrm{miss}}$. As shown in the previous section, we expect to see a reduced number of tau leptons though, depending on $\mathrm{BR}_{\mathrm{cl}}$.

In order to get a better sense of how the signals compare, let's look at the distributions of the relevant variables and object multiplicities. We will first compare a stop-stau signal with $(m_{\tilde{t}}, m_{\tilde{\tau}}) = (750, 590)$ GeV to the nominal LQ_3 samples ($\beta = 0.5$) of $\mathrm{LQ}_3^{\mathrm{u}}$ and $\mathrm{LQ}_3^{\mathrm{d}}$ with $m_{\mathrm{LQ}} = 750$ GeV and keep in mind that the distributions may vary for other β (or $\mathrm{BR}_{\mathrm{cl}}$). When appropriate, we will decompose the nominal samples into their three classes, defined by $n_{\mathrm{cl}} = 0, 1, 2$, which is similar to showing the effect of varying $\mathrm{BR}_{\mathrm{cl}}$.

Table 4.7 shows the yields for the three benchmark signals after lep-had and had-had preselections, broken down by the number of charged leptons in the final state n_{cl} for the leptoquark signals. As we only consider strong production mechanisms for both LQ_3 and stop-stau signals and since both are scalar color-triplets, the production cross-sections are the same for equal masses. Therefore, we can see from the total number of events that passed the preselections that, as expected, the requirements are much less suited for LQ_3 than for stop-stau. We observe that the preselections favor $n_{cl} = 2$ and reject almost all events without charged leptons ($n_{cl} = 0$) due to the lepton requirements. $\mathrm{LQ}_3^{\mathrm{u}}$ has a small contribution from $n_{\mathrm{cl}} = 0$ events, in which leptons from the top decay can be selected. For $\mathrm{LQ}_3^{\mathrm{d}}$, the events with leptons coming from the bottom decay cannot be selected, since the overlap removal procedure removes one of the objects[6] and if both leptons have to emerge from the b-quarks, either the jet or the lepton requirement cannot be fulfilled. We also observe that $n_{\mathrm{cl}} = 1$ events contribute substantially in lep-had, but only marginally in had-had. In $\tau t \nu b$ events, we have to rely on the top quark or another source to get the second lepton. Since it is much less likely that a top quark decays into a tau lepton that further decays hadronically, than the decay directly or through a tau lepton into a light lepton, the lep-had channel has a higher chance of accepting these events. The $\mathrm{LQ}_3^{\mathrm{d}}$ yield in had-had is very small, even for events where $n_{\mathrm{cl}} = 2$. This is mainly due to the lepton veto, which discards about 40% of those events, which can be seen in figure 4.4, which shows the efficiency of different cuts leading to the had-had preselection for LQ_3 signals with $\mathrm{BR}_{\mathrm{cl}}$=1 and a stop-stau signal. The lepton veto is triggered by additional leptons coming from the decay of the top quarks in $t\tau t\tau$ final states.

Now let's discuss the variables used to define the signal regions, using the same benchmark signals. The top two plots of figure 4.5 show the m_{T2} distributions with lep-had and had-had preselections, respectively. We see that, compared to the stop-stau signal, $\mathrm{LQ}_3^{\mathrm{u}}$ and $\mathrm{LQ}_3^{\mathrm{d}}$ have much more events with low m_{T2}. Since we require at least 80 GeV in the lep-had channel and 100 GeV in had-had channel, these events will not contribute in the signal regions. From the plots beneath on the same figure, where we split the contributions from different classes of events, defined by n_{cl}, we see that the events with low m_{T2} mostly come from $n_{\mathrm{cl}} = 2$ events, while the distribution is much flatter for $n_{\mathrm{cl}} = 1$ events. So this variable seems not to be well suited for final states $[q, \tau]$,$[q, \tau]$. Indeed, the goal of m_{T2} is to distribute the total $E_{\mathrm{T}}^{\mathrm{miss}}$ between the selected leptons and calculate their transverse mass, in order to get high values for signals containing heavy particles. Here, there are no prompt neutrinos. For $n_{\mathrm{cl}} = 1$ events, with final states $[q, \tau][q', \nu]$, there is a prompt neutrino and m_{T2} yields higher values. As can be seen in figure 4.6, for a sizable number of $\mathrm{LQ}_3^{\mathrm{d}}$ events, the selected leptons are not

[6]Since the bottom quark is relatively light, its decay products are almost collinear.

	Lep-Had			
Signal	$n_{cl} = 0$	$n_{cl} = 1$	$n_{cl} = 2$	total (raw)
LQu 750	0.45 ± 0.18	22.53 ± 1.54	28.02 ± 1.95	$51.0 \pm 2.5(1614)$
LQd 750	0.0 ± 0.0	19.26 ± 1.57	26.8 ± 1.75	$46.07 \pm 2.36(1476)$
SS (750,590)				$82.81 \pm 2.54(1544)$
	Had-Had			
Signal	$n_{cl} = 0$	$n_{cl} = 1$	$n_{cl} = 2$	total (raw)
LQu 750	0.0 ± 0.0	3.97 ± 0.7	28.47 ± 1.85	$32.45 \pm 1.97(936)$
LQd 750	0.0 ± 0.0	4.96 ± 0.62	14.4 ± 1.44	$19.36 \pm 1.57(606)$
SS (750,590)				$96.87 \pm 2.97(1648)$

Table 4.7: Event yields with statistical uncertainties after applying the preselection cuts for LQ_3^u and LQ_3^d with $m_{LQ} = 750$ GeV and $\beta = 0.5$ and a stop-stau signal with $(m_{\tilde{t}}, m_{\tilde{\tau}}) = (750, 590)$ GeV. For the LQs, the yields are also given as a function of n_{cl}. The number of raw events is given in brackets.

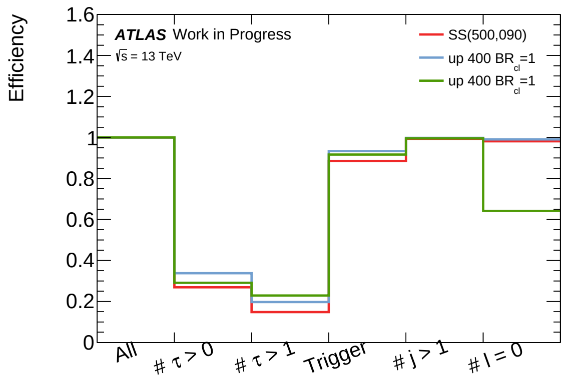

Figure 4.4: Efficiency cutflow from left to right for the had-had preselection. LQ_3^u in blue and LQ_3^d in green with $m_{LQ} = 400$ GeV and $BR_{cl} = 1.0$. Stop-stau with $(m_{\tilde{t}}, m_{\tilde{\tau}}) = (500, 090)$ GeV in red. Every bin shows the efficiency of the cut w.r.t to the number of events remaining after applying all previous cuts (to the left). The first bin contains all events, as calculated from the production cross-section and the integrated luminosity. The fourth bin accepts events for which the required trigger fired and the trigger plateau is reached.

of opposite sign. These are almost exclusively $n_{\text{cl}} = 2$ events and show that for some events, the prompt leptons failed to be reconstructed and a lepton from the top decay was selected. This is not the case for LQ_3^u. As already discussed, these events would be rejected due to overlap removal.

The remaining distributions of the variables used for the definition of the signal regions are shown in figure 4.7. As we see, LQ_3 signals show similar shapes to stop-stau signals. For these variables, all classes of events have similar distributions.

Table 4.8 shows the yields in the signal regions for the same benchmark signals, broken down by the number of charged leptons in the final state n_{cl} for the leptoquark signals. Now clearly events with $n_{\text{cl}} = 1$ are favored and we lose most of the $n_{\text{cl}} = 2$ events. We understand that most of these events are discarded due to low m_{T2} values.

Now let's see how the benchmark signals compare to the backgrounds. Figures 4.8 and 4.9 show the distributions of variables used for the SR requirements, where all cuts are applied,

	LH SR			
Signal	$n_{cl} = 0$	$n_{cl} = 1$	$n_{cl} = 2$	total (raw)
LQu 750	0.22 ± 0.1	6.91 ± 0.88	0.09 ± 0.06	$7.23 \pm 0.89(219)$
LQd 750	0.0 ± 0.0	5.54 ± 0.85	0.56 ± 0.2	$6.1 \pm 0.88(233)$
SS (750,590)				30.78(583)
	HH SR			
Signal	$n_{cl} = 0$	$n_{cl} = 1$	$n_{cl} = 2$	total (raw)
LQu 750	0.0 ± 0.0	1.95 ± 0.52	0.71 ± 0.25	$2.66 \pm 0.58(58)$
LQd 750	0.0 ± 0.0	1.35 ± 0.31	0.53 ± 0.21	$1.88 \pm 0.38(51)$
SS (750,590)				58.86(980)

Table 4.8: Event yields with statistical uncertainties after applying the signal region cuts for $\mathrm{LQ}_3^{\mathrm{u}}$ and $\mathrm{LQ}_3^{\mathrm{d}}$ with $m_{\mathrm{LQ}} = 750$ GeV and $\beta = 0.5$ and a stop-stau signal with $(m_{\tilde{t}}, m_{\tilde{\tau}}) = (750, 590)$ GeV For the LQs, the yields are also given depending on the truth variable n_{cl}. The number of raw events is given in the brackets.

except the one for which the distribution is plotted. Vertical lines show where the final cut is to be applied. The bottom panel shows the significance Z that one would obtain by applying the cut at any given value. Besides the fact that a lot of LQ_3 events have low values of m_{T2}, the variables discriminate well between background. Although using the variable m_{T2} might not be optimal for LQ_3 signals, the values of the cuts are close to optimal.

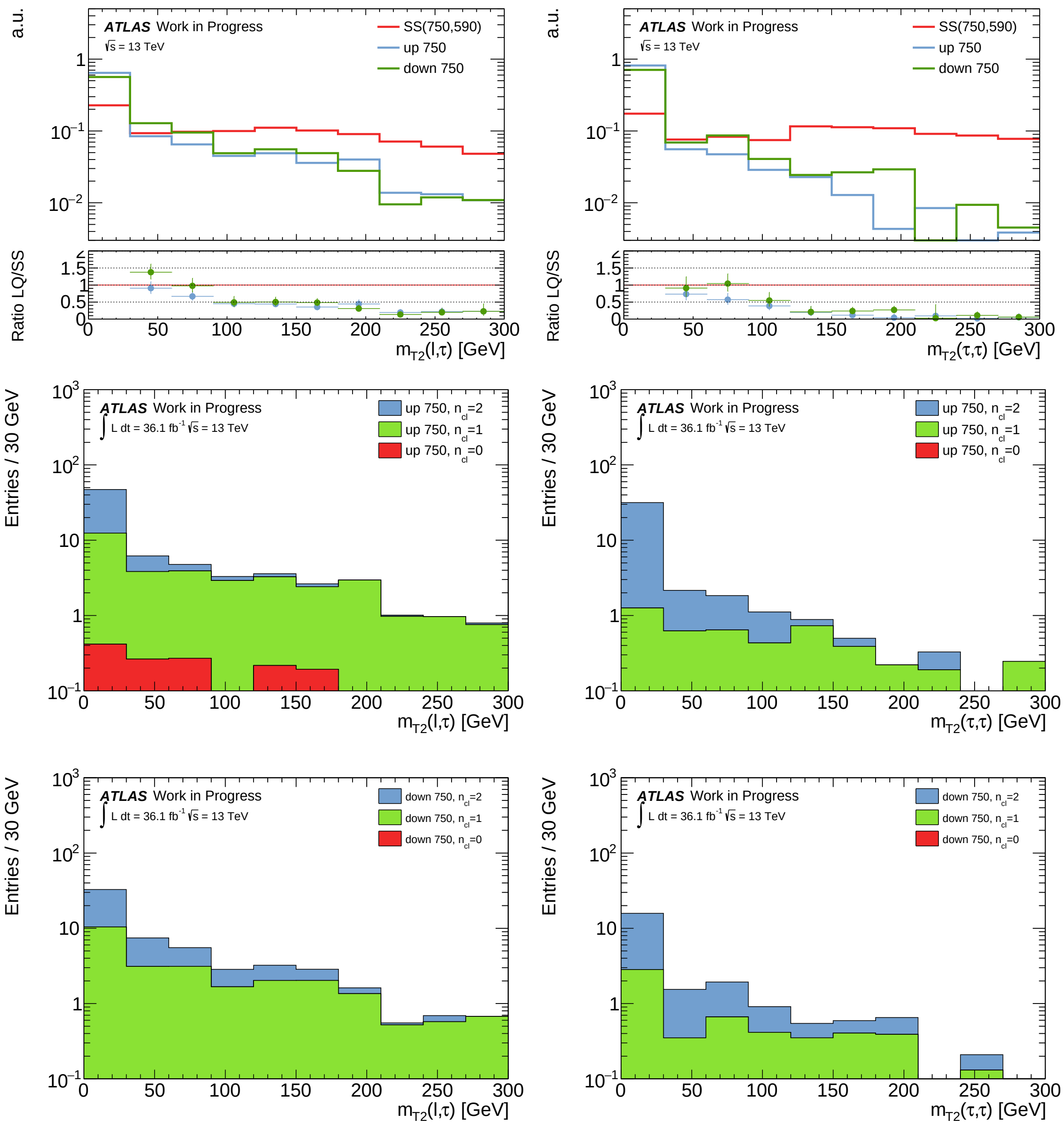

Figure 4.5: Distributions of the variables m_{T2} in the lep-had (left) and had-had (right) preselections. The top two plots show normalized distributions that compare $\mathrm{LQ}_3^{\mathrm{u}}$ and $\mathrm{LQ}_3^{\mathrm{d}}$ with m_{LQ}= 750 GeV and a stop-stau signal with $(m_{\tilde{t}}, m_{\tilde{\tau}}) = (750, 590)$ GeV for the lep-had (left) and had-had (right) preselections. Below, $\mathrm{LQ}_3^{\mathrm{u}}$ and $\mathrm{LQ}_3^{\mathrm{d}}$ are shown separately in lep-had (left) and had-had (right), with each color representing a class of events defined by the number of charged leptons in the final states.

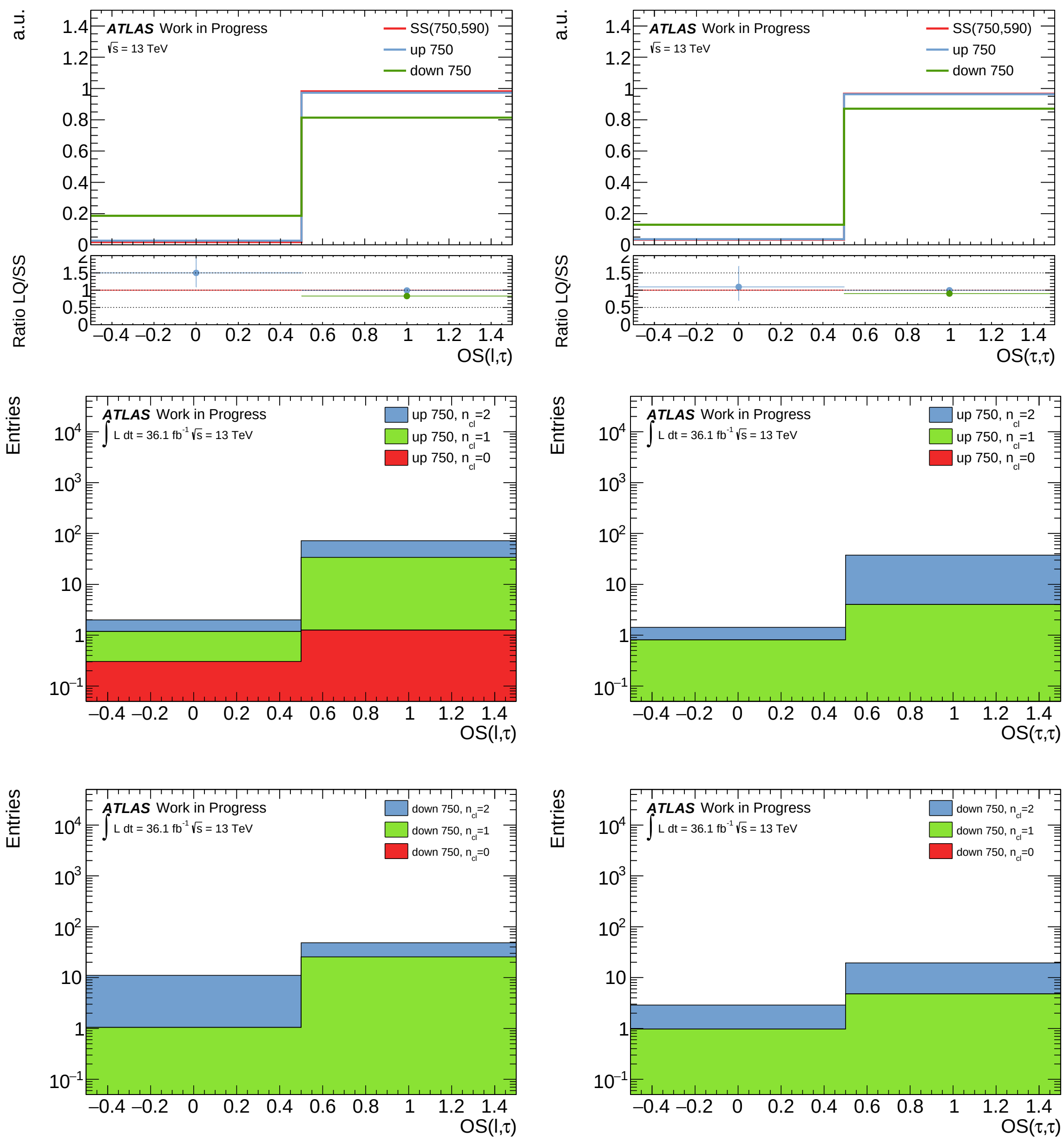

Figure 4.6: Distributions of the variable OS, which takes the value 1 when the selected leptons are of opposite sign and 0 otherwise, in the lep-had (left) and had-had (right) preselections. The top two plots show normalized distributions that compare $\mathrm{LQ}_3^{\mathrm{u}}$ and $\mathrm{LQ}_3^{\mathrm{d}}$ with m_{LQ}= 750 GeV and a stop-stau signal with $(m_{\tilde{t}}, m_{\tilde{\tau}}) = (750, 590)$ GeV for the lep-had (left) and had-had (right) preselections. Below, $\mathrm{LQ}_3^{\mathrm{u}}$ and $\mathrm{LQ}_3^{\mathrm{d}}$ are shown separately in lep-had (left) and had-had (right), with each color representing a class of events defined by the number of charged leptons in the final states.

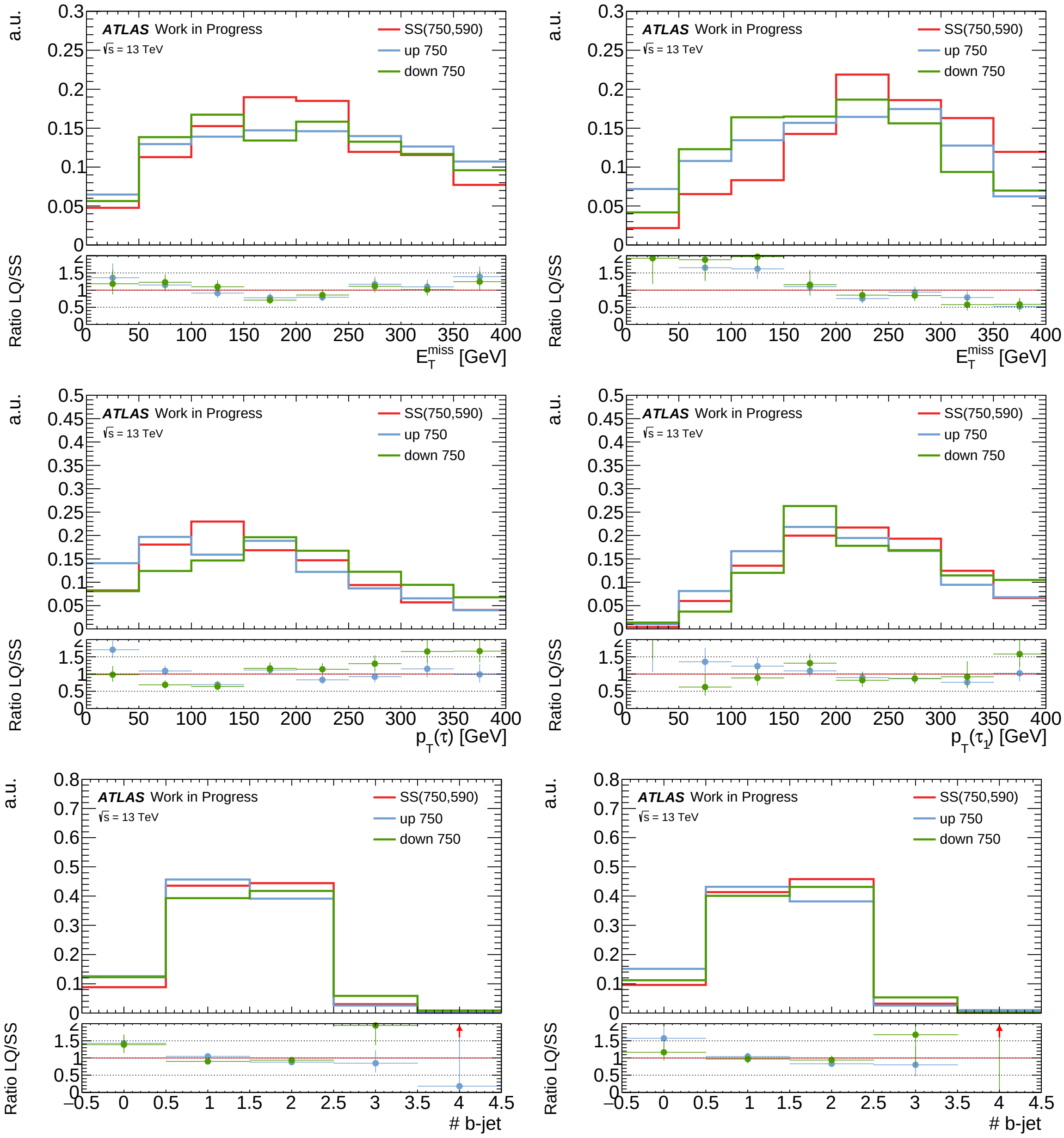

Figure 4.7: Comparisons between a LQ_3^u signal and a LQ_3^d signal with $m_{LQ} = 750$ GeV and $\beta = 0.5$ and a stop-stau signal with $(m_{\tilde{t}}, m_{\tilde{\tau}}) = (750, 590)$ GeV in the lep-had channel (left) and had-had channel (right), after applying the respective lep-had / had-had preselection. All distributions are normalized to unity. The plots in the bottom panels show the ratio of the LQ signals w.r.t. the stop-stau signal with error bars indicating the statistical uncertainties.

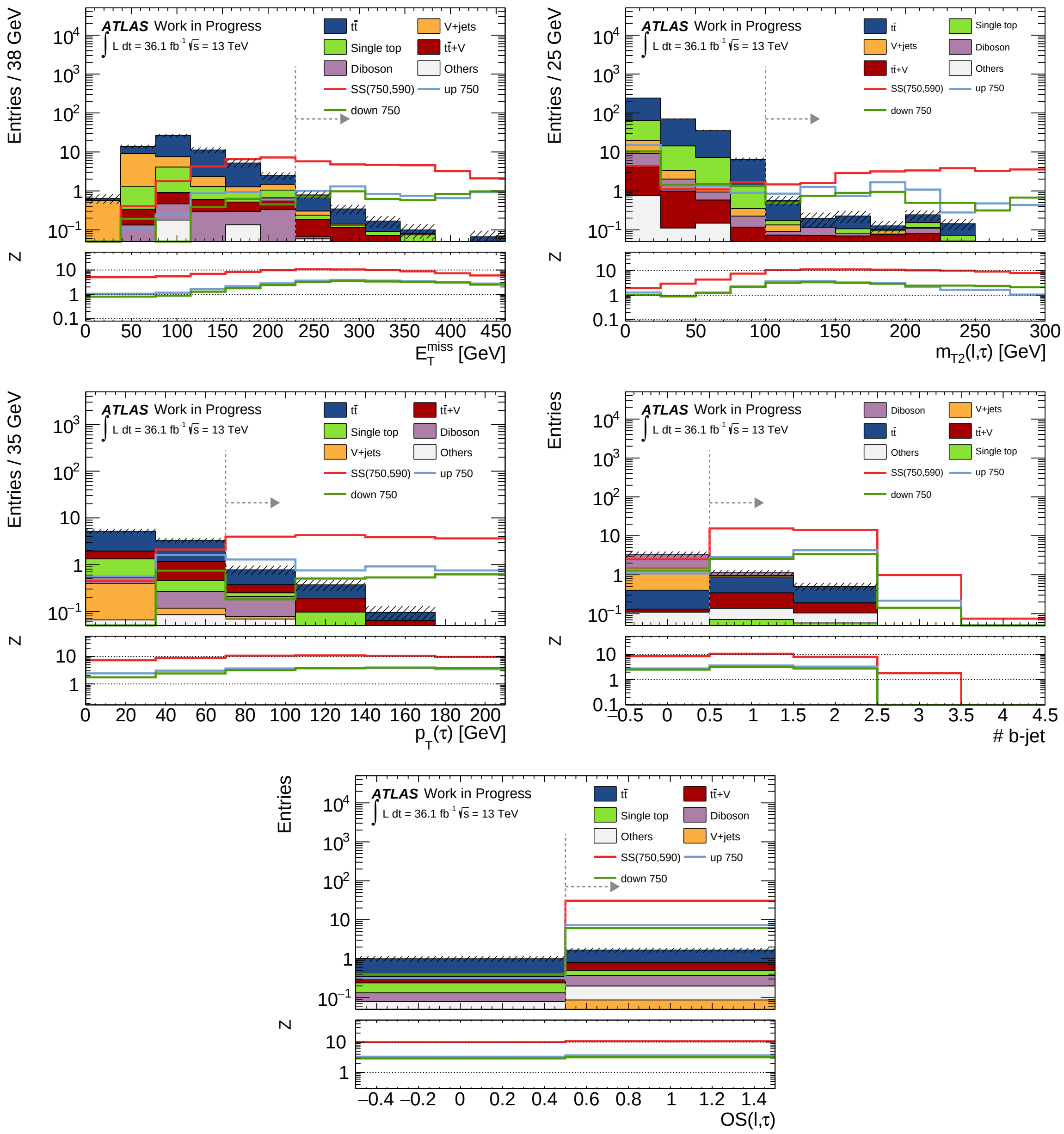

Figure 4.8: Distributions of variables used for the definition of SR LH for $\mathrm{LQ}_3^{\mathrm{u}}$ and $\mathrm{LQ}_3^{\mathrm{d}}$ with $\beta = 0.5$ and m_{LQ}= 750 GeV, a stop-stau signal with $(m_{\tilde{t}}, m_{\tilde{\tau}}) = (750, 590)$ GeV and the nominal background expectations before normalization. The diagonal lines show the total statistical uncertainties on the background. All signal selections are applied except for the one shown in the plot. The vertical, dashed, grey lines show where the final cut is to be applied and the arrows indicate whether it is a lower or upper boundary. The bottom panels show the significance Z one would obtain by applying the cut at the lower bin boundary.

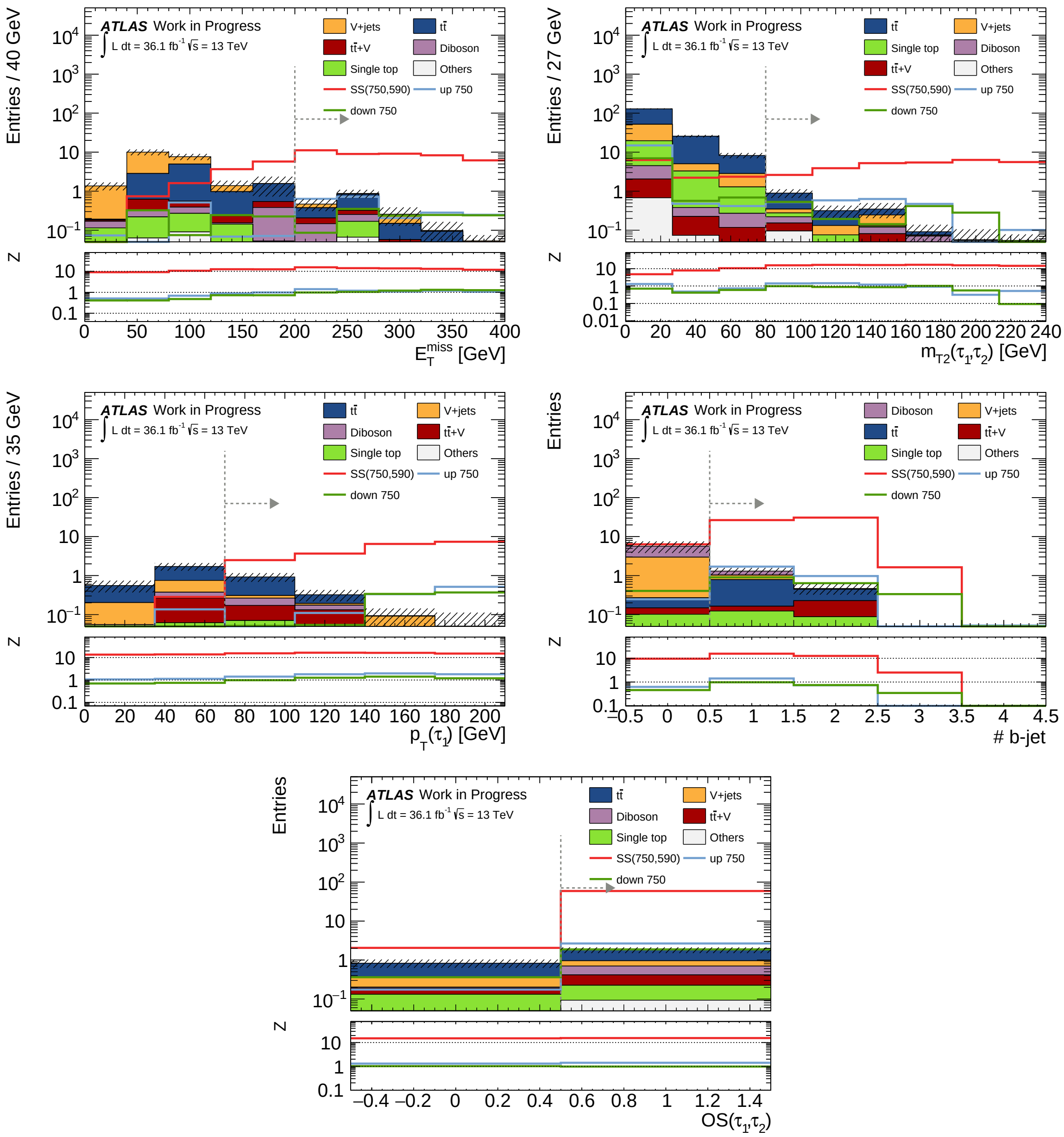

Figure 4.9: Distributions of variables used for the definition of SR HH for $\mathrm{LQ}_3^{\mathrm{u}}$ and $\mathrm{LQ}_3^{\mathrm{d}}$ with $\beta = 0.5$ and m_{LQ}= 750 GeV, a stop-stau signal with $(m_{\tilde{t}}, m_{\tilde{\tau}}) = (750, 590)$ GeV and the nominal background expectations before normalization. The diagonal lines show the total statistical uncertainties on the background. All signal selections are applied except for the one shown in the plot. The vertical, dashed, grey lines show where the final cut is to be applied and the arrows indicate whether it is a lower or upper boundary. The bottom panels show the significance Z one would obtain by applying the cut at the lower bin boundary.

4.5 Results and discussion

Table 4.9 shows the observed number of events in the signal regions, together with the SM expectation and the expected yields for a couple of signals. We see that in both channels, the observation fits the SM expectation and seems only to yield a slight upward fluctuation. A discovery is hereby not to be considered. Now the question is to which extent the LQ_3 models are excluded. It seems already clear that e.g. LQu with m_{LQ}= 500 GeV and $\mathrm{BR}_{\mathrm{cl}}$, for which we would expect about 11 events in SR HH and 27 events in SR LH, can be excluded with high significance. In order to quantify the exclusion we use the statistical methods described in section 3.5. Namely, we use the CL_s method with the profile likelihood ratio as a test statistic and fit the number of events in both signal regions simultaneously. We call the fit where we use both signal regions as *combined* fit. The results of individual channels will also be used later.

		SR HH		SR LH	
Observed events		2		3	
Total SM		1.9 ± 1.0		2.2 ± 0.6	
	σ [pb]	Yield $\pm\sigma_{stat}$	ϵ [%]	Yield $\pm\sigma_{stat}$	ϵ [%]
$\mathrm{up}^{0.5}_{500}$	0.483	10.8 ± 2.5	0.06	26.7 ± 4.1	0.15
$\mathrm{up}^{0.0}_{750}$	0.043	0.0 ± 0.0	0.0	1.0 ± 0.2	0.06
$\mathrm{up}^{0.5}_{750}$	0.043	2.6 ± 0.6	0.17	7.3 ± 0.9	0.47
$\mathrm{up}^{1.0}_{750}$	0.043	2.5 ± 0.5	0.16	0.3 ± 0.1	0.02
$\mathrm{up}^{0.5}_{1000}$	0.006	0.3 ± 0.1	0.13	1.1 ± 0.1	0.49
$\mathrm{down}^{0.5}_{500}$	0.483	24.6 ± 3.8	0.14	49.1 ± 5.6	0.28
$\mathrm{down}^{0.0}_{750}$	0.043	0.0 ± 0.0	0.0	0.0 ± 0.0	0.0
$\mathrm{down}^{0.5}_{750}$	0.043	1.9 ± 0.4	0.13	6.2 ± 0.9	0.4
$\mathrm{down}^{1.0}_{750}$	0.043	2.4 ± 0.5	0.15	2.5 ± 0.4	0.16
$\mathrm{down}^{0.5}_{1000}$	0.006	0.5 ± 0.1	0.24	1.6 ± 0.2	0.74

Table 4.9: The number of observed events and expected background events in SR HH and SR LH, together with the number of expected signal events for different LQ types, masses (lower index) and branching ratios into charged leptons (upper index). Signal cross sections σ and signal efficiencies ϵ are also given.

We have seen in section 2.3, that theoretically, $\beta =$ should take values of 0, 1 or 1/2. We therefore start by examining an upper limit scan for $\beta = 0.5$, for which we have good sensitivity. This result is shown in figure 4.10. At the theoretically predicted cross-section, we exclude $\mathrm{LQ}_3^{\mathrm{u}}$ up to about 780 GeV and $\mathrm{LQ}_3^{\mathrm{d}}$ up to 800 GeV. The fact that the observed excluded cross-sections are higher than the expected excluded cross-section is related to the fact that we observed slightly more events than we expected. Therefore a potential signal contribution is slightly more likely as expected from the SM. We interpret the fluctuations in the exclusion limits as statistical fluctuations in the Monte-Carlo simulations.

It is also interesting to see how each channel performs individually. This is shown in figure 4.11. We see that the lep-had yields much higher exclusion limits. The limits on the theoretically predicted cross-sections are only about 20 GeV lower than for the combined fit. This can also be understood when looking at the signal yields in the SRs shown in table 4.9, where we see that the expected number of events for $\mathrm{BR}_{\mathrm{cl}}$= 0.5 is much higher in the lep-had SR than in the had-had SR. The reason for this, as shown in the previous section in figure 4.5, is that LQ_3 signals yield a lot more events with very low m_{T2} in the had-had channel than in the lep-had channel.

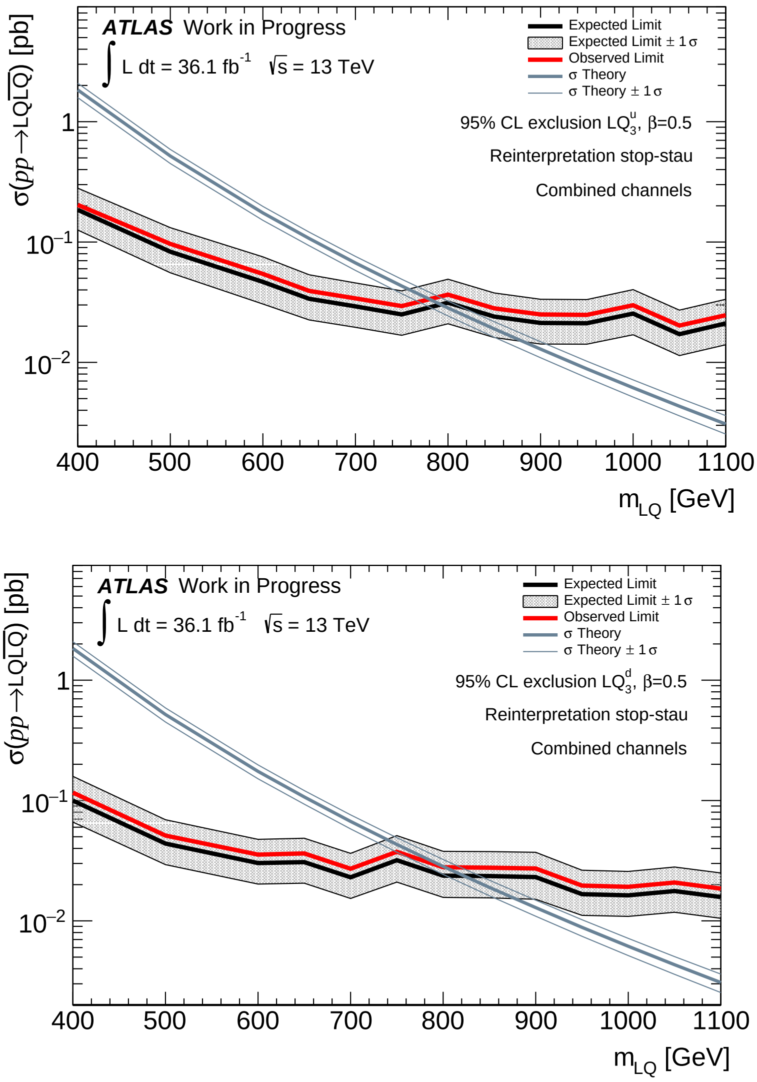

Figure 4.10: Expected (black) and observed (red) excluded signal cross-sections for $\beta = 0.5$ at 95 % CL as a function of the leptoquark mass. The uncertainty on the expected limit includes all systematic and statistical uncertainties. The theoretical signal cross-section (thin black lines) and its uncertainty are also shown. $\mathrm{LQ}_3^{\mathrm{u}}$ is shown on top and $\mathrm{LQ}_3^{\mathrm{d}}$ below. The combined fit was used.

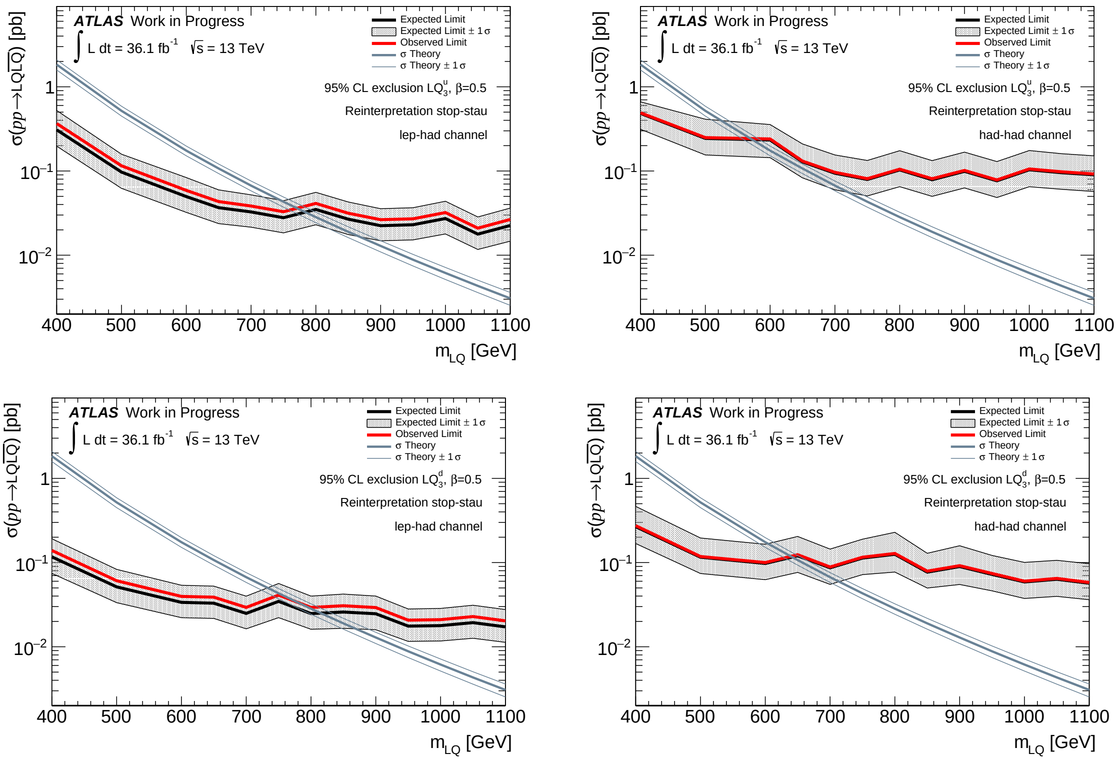

Figure 4.11: Same plots as in 4.10 but for the lep-had channel (left) and had-had channel (right) individually.

We also want to see to which extend we exclude LQ_3 models with other values of β. This can be seen in figure 4.12, which shows the exclusion limits for both signal models in the m_{LQ}-BR_{cl} plane at 95% CL. Now an uncertainty on the observed limit is also included. It is calculated from the theoretical uncertainty on the signal cross-section. We see that for both models, exclusion is maximal at BR_{cl} near 0.5 and drops off rapidly at BR_{cl}=0, where there are no more charged leptons from the hard process.

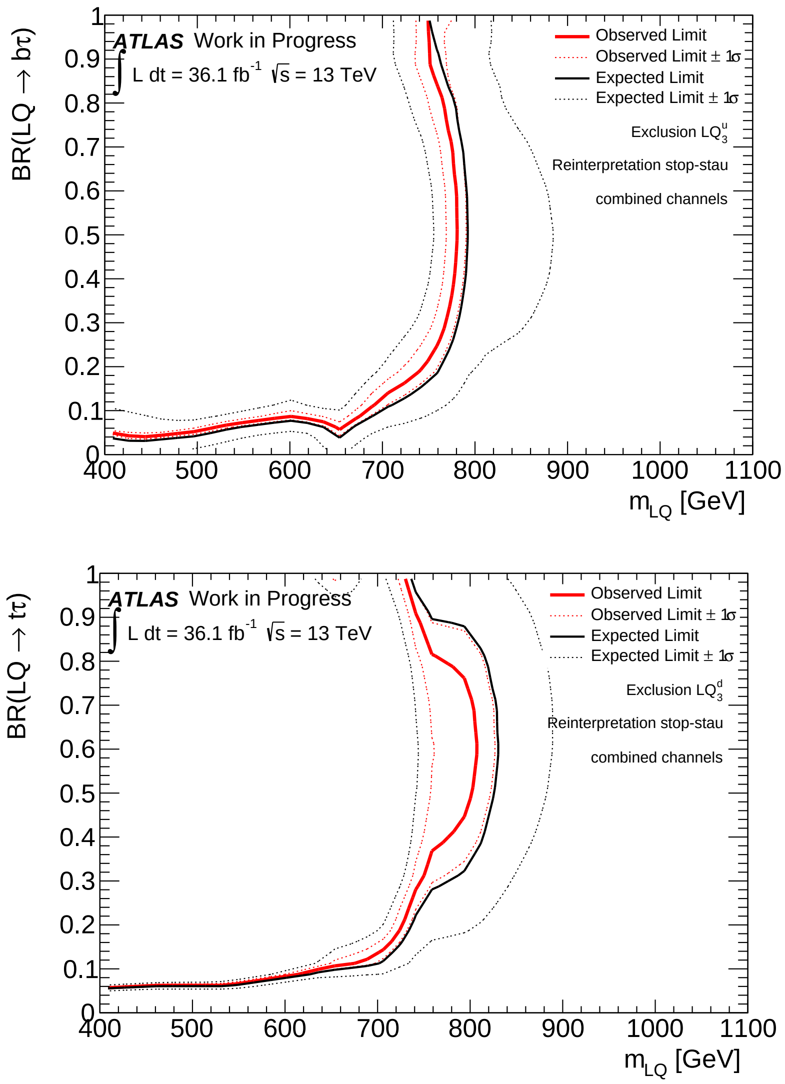

Figure 4.12: Expected (black) and observed (red) exclusion reach at 95 % CL in the m_{LQ3}–BR_{cl} plane obtained from the combined fit. The uncertainties on the observed limit is obtained from the theoretical uncertainty on the signal cross-section. They correspond to the uncertainty bands given for the theoretical uncertainty in the upper limit scans of figures 4.10 and 4.11.

4.5.1 Signal contamination in control regions

The CRs for $t\bar{t}$ in both channels suffer from significant signal contamination. Figures 4.13 and 4.14 show the signal contamination in each CR in terms of percentage to the total background for $\mathrm{LQ}_3^{\mathrm{u}}$ and $\mathrm{LQ}_3^{\mathrm{d}}$, respectively. The reason for such high signal contamination is again related to low values of m_{T2}, which is a requirement in the definition of the $t\bar{t}$ CRs. As discussed in section 4.4, most events with low values of m_{T2} are $[q,\tau][q,\tau]$ events. Therefore, high $\mathrm{BR}_{\mathrm{cl}}$ signals are most affected. We do account for signal contamination in the likelihood. Therefore, the statistical model should still be valid. Nonetheless, some consequences should be discussed.

- Numerical methods, which are used in e.g. the minimization of the likelihood, tend to fail when there is a lot of signal contamination. This could be an indication that the fit is unstable because of an unusual shape of the likelihood. Even if the fitting procedure succeeds, the validity of the result is questionable if the fit is unstable.
- If signal was contributing to data in CRs, then the background-only fit is not a valid measurement of the background. This should be noticed in the VRs if the signal contamination is high, except if the signal also contributes in the VRs by a comparable amount relative to the background.
- The normalization of the background is affected, especially in the maximum likelihood used in the numerator of the likelihood ratio 3.3 for a signal strength $\mu = 1$. For example, the $t\bar{t}$ *fake* contribution is fitted to 0 for the fit including $\mathrm{LQ}_3^{\mathrm{u}}$ with m_{LQ}=400 GeV and $\mathrm{BR}_{\mathrm{cl}}$=1. Even if the statistical model is correct, the CRs do not fulfill their purpose, which is controlling the background. Since these CRs accept a lot of signal events, they should rather be considered as SRs than CRs.
- The CL_s method is advertised as quantifying the likelihood of the measurement under the H_{s+b} hypothesis, compared to the likelihood of the measurement under H_b. But the p-value $p(\mu = 0)$ is not independent of the signal model, as the denominator of the likelihood ratio is the maximum likelihood obtained with a fitted signal strength. It can be questioned whether it is healthy to calculate $p(\mu = 0)$ with background models which substantially differ from the models obtained from the background-only fit. Fortunately, the effect on the normalization factors in the fits with free signal strength parameters is small, as will be shown later. So the background models obtained for the calculation of p_b are not so different from the models obtained in a background-only fit.

4.5.2 Mitigation of signal contamination

In order to not mistakenly claim that a signal is excluded, we chose to not include signal points in the exclusion plots if there is a CR with more than 30% signal contamination. But we see from figures 4.13 and 4.14 that for a lot of signal points, only CRs in the had-had channel are significantly affected by signal contamination. For these points we can still use the result of the lep-had channel, which is stronger anyway. With this strategy we obtain the exclusion plots of figure 4.15.

The choice of the threshold is arbitrary, but we have to make a choice if we want to limit signal contamination. 30% seems quite reasonable, since with this amount of signal contamination, the backgrounds are normalized to values that stay within the 1 σ uncertainties of the value estimated by the background-only fit. The relationship between signal contamination in $t\bar{t}$ CRs and the normalization of $t\bar{t}$ backgrounds can be seen in figures 4.16 to 4.19. The relationship is shown for the combined fit with free signal strength in figure 4.16 and the

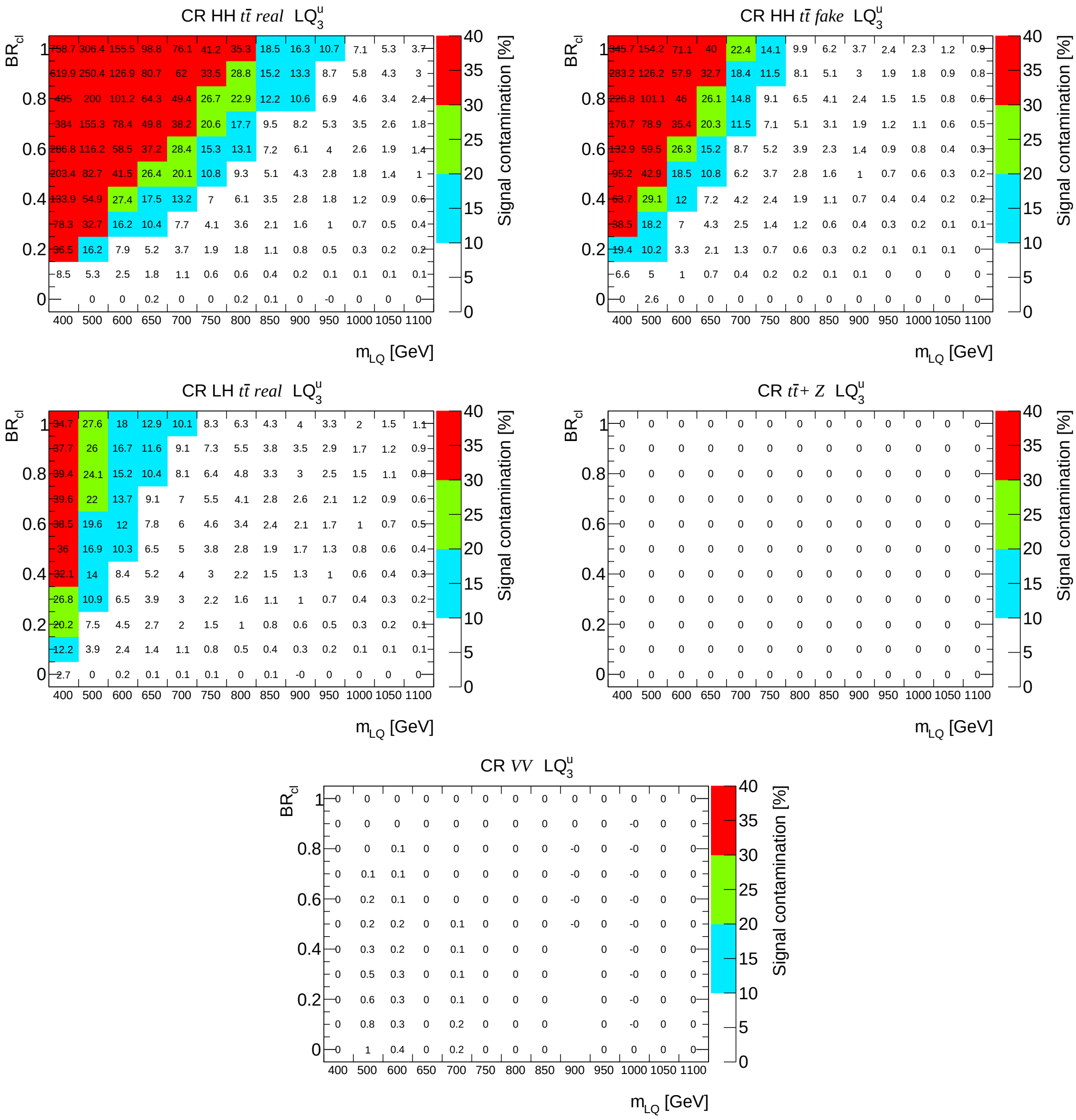

Figure 4.13: Signal contamination in all control regions for LQ_3^u. The contamination is given in terms of the ratio of expected signal events over the post-fit background yields from the background-only fit in percent.

signal strength fixed at one in figure 4.17. The fit in the lep-had channel is shown in figure 4.18 for free signal strengths and figure 4.19 for fixed signal strength. In these plots, every point corresponds to a signal point from the 2-D grid of LQ_3 models. The color of the dots classifies signal points with respect to the signal contamination with a threshold of 30%. Green dots are signals for which no CR in any channel is affected by a contamination higher than the threshold and for which we therefore use the combined fit. Yellow dots are signals for which a CR in the had-had channel is affected above the threshold, but where no CR in the lep-had channel is affected that much, such that we can still use the lep-had result. Red dots show the points for which, in both channels, there is a CR which is affected above the threshold, which means that we do not include them in the exclusion plots. Also shown in these plots is the background expectation and its uncertainty from the background-only fit. We observe that the background expectation is not affected that much for fits with a free signal strength (figure 4.16). This makes sense, since we can scale the signal down instead of the background, in order to fit the total number of events to the observed number of events,

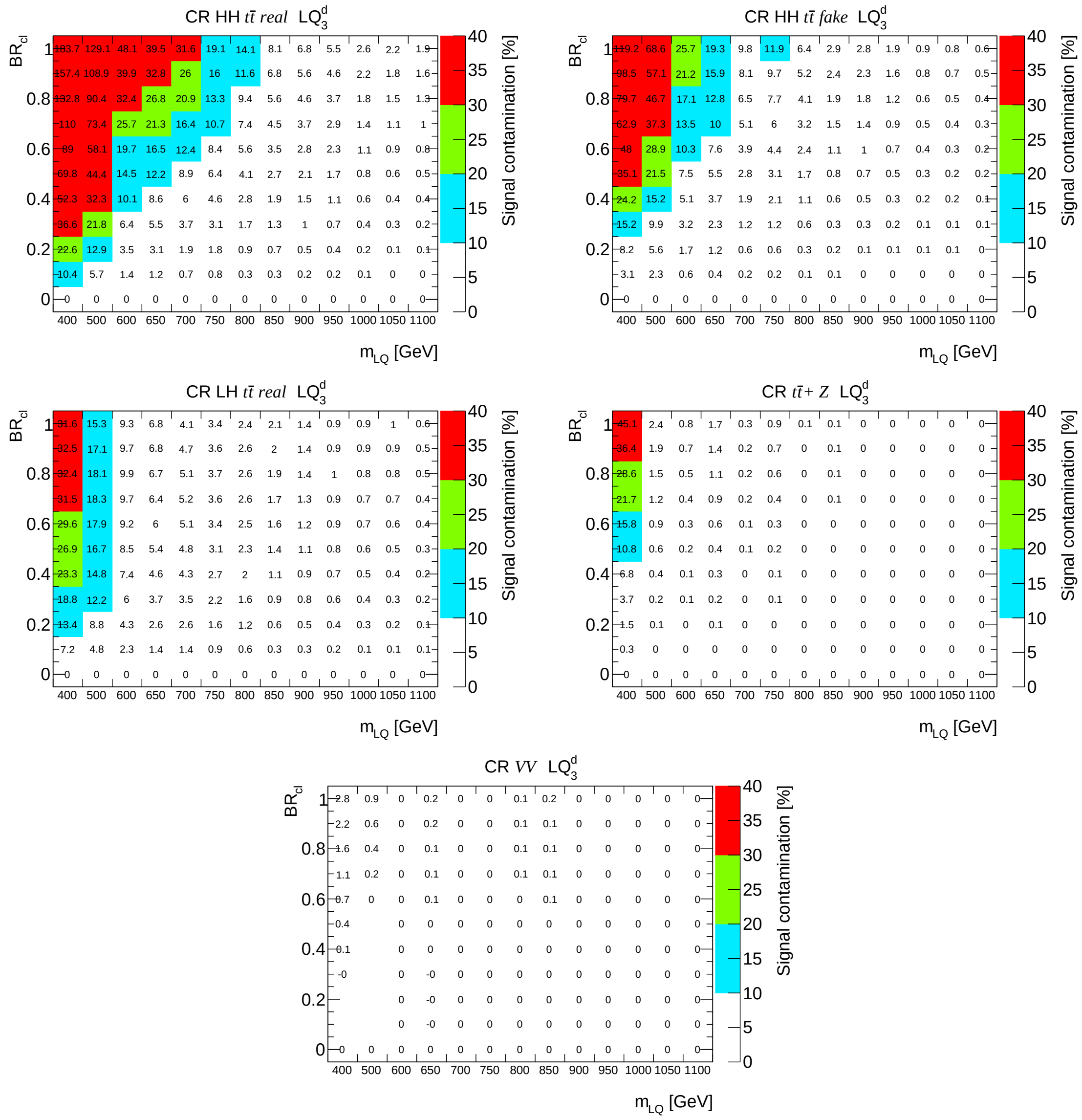

Figure 4.14: Signal contamination in all control regions for LQ_3^d. The contamination is given in terms of the ratio of expected signal events over the post-fit background yields from the background-only fit in percent.

whereas for fits with fixed signal strengths, we are obliged to scale down the background. Only in the lep-had fit (figure 4.18), the $t\bar{t}$ *real* background may be fitted outside its uncertainty, even with free signal strength. Some investigation is needed to understand this, but these points are of limited interest for our final result, since the signal yields of these points in the lep-had SR are too low for them to be excluded anyways. We also see that the choice of 30% as a threshold is justified. Indeed, although some points in the plots of figure 4.17 are outside the uncertainty band, these are all red (or green) dots, for which we will use the lep-had result. All black dots on this figure are within the uncertainty of the background. For red dots we look at figure 4.19. There, only few red points are outside the uncertainty of the background.

An alternative way to get around signal contamination, would be to do upper limit scans. Indeed, if we can show that we can exclude a signal with a reduced production cross-section, then also the signal contamination in the CR is reduced. But at this point we should mention that the problematic region of the parameter space (low LQ masses and high BR_{cl}) is not a region that we should be particularly concerned about, because other 13 TeV ATLAS analysis exclude this region, as will be shown below.

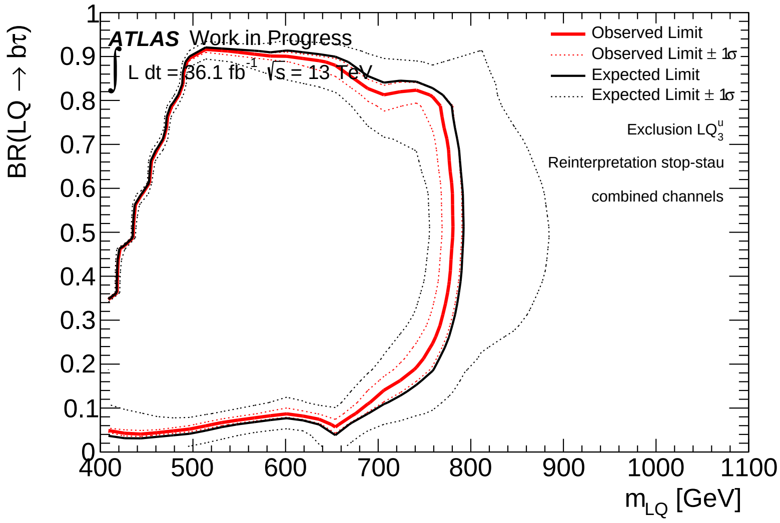

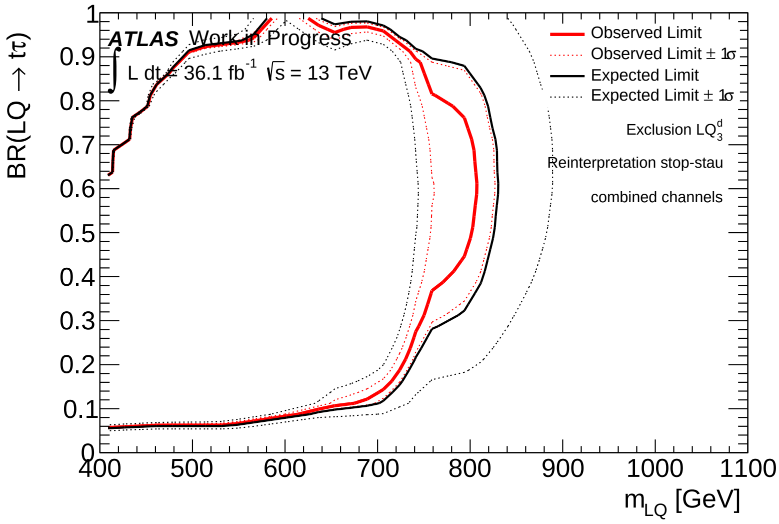

Figure 4.15: Same plot as in Figure 4.12, but taking into account signal contamination and following the recipe described above.

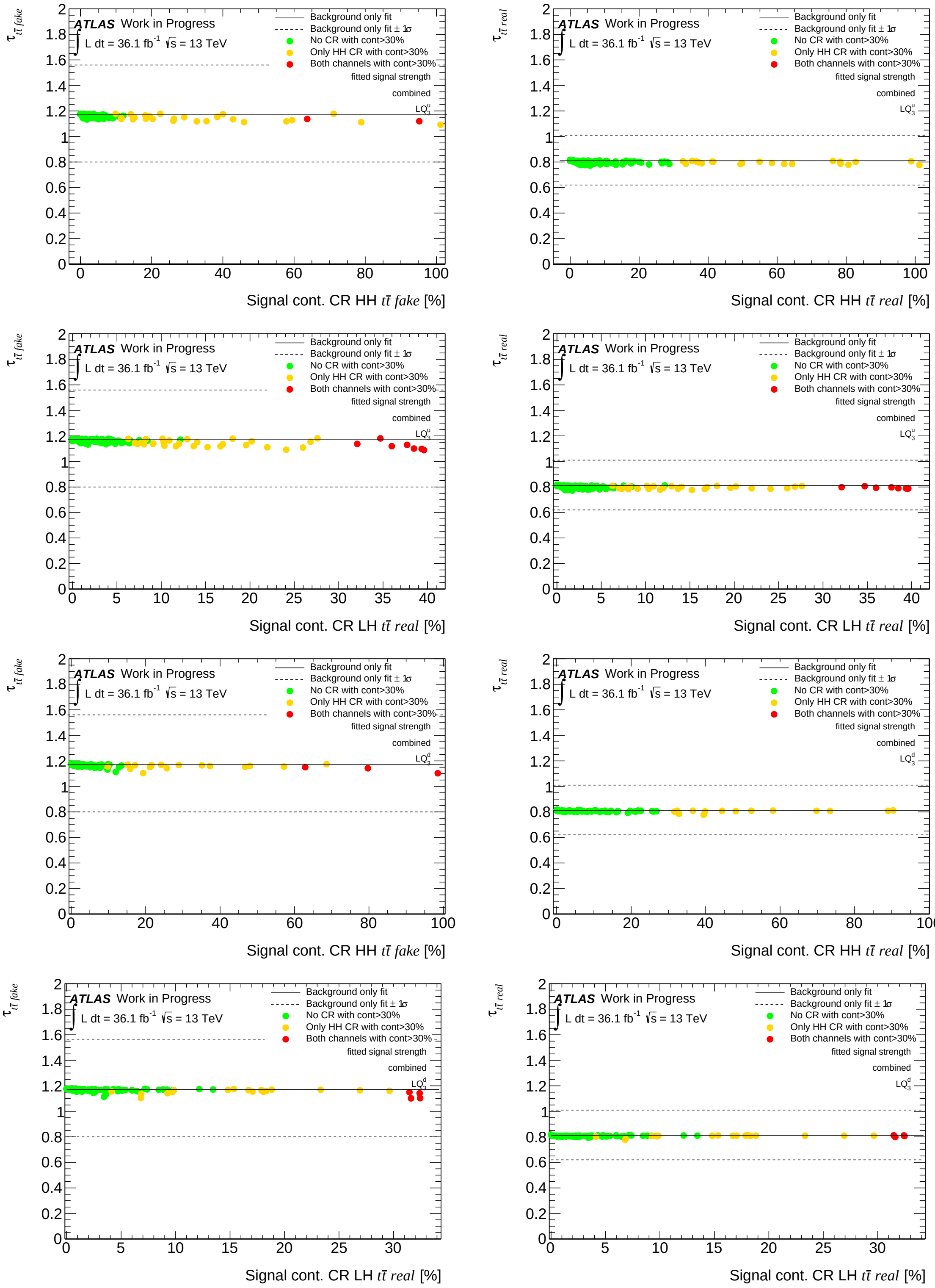

Figure 4.16: Scatter plots for the signals of $\mathrm{LQ}_3^{\mathrm{u}}$ (top 4) and $\mathrm{LQ}_3^{\mathrm{d}}$ (bottom 4) showing the effect of signal contamination on the normalization factors τ for the $t\bar{t}$ *real* and $t\bar{t}$ *fake* backgrounds. These are combined fits with floating signal strengths. The horizontal lines show the normalization factors from the background-only fit with $\pm 1\sigma$ uncertainties. Green dots are signal points where no CR has more than 30 % contamination. Yellow dots are points where only had-had regions have more than 30 % signal contamination. Red dots have at least a control region in each channel with more than 30 % signal contamination.

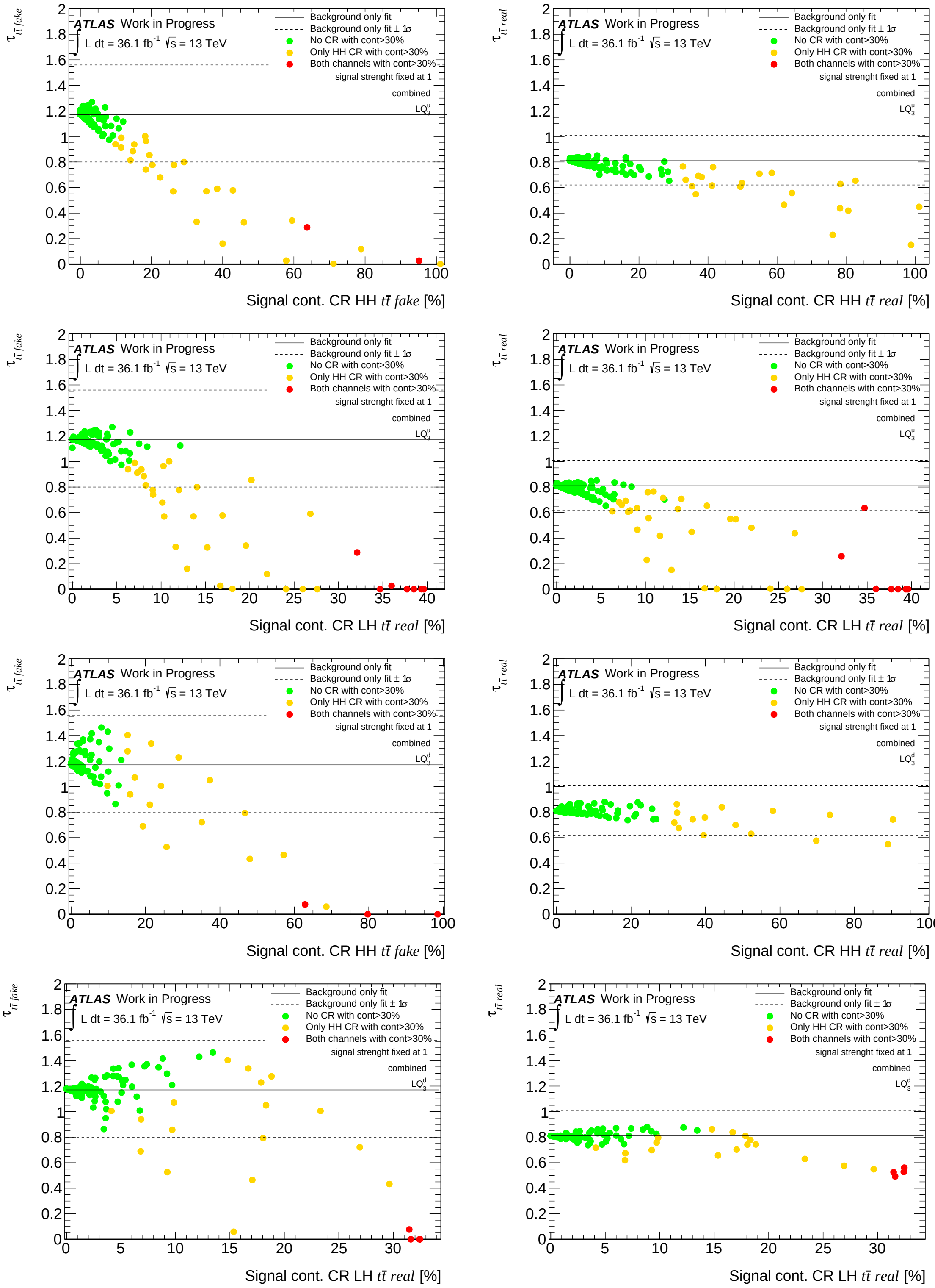

Figure 4.17: Same plots as in figure 4.16, but with signal strengths fixed at one.

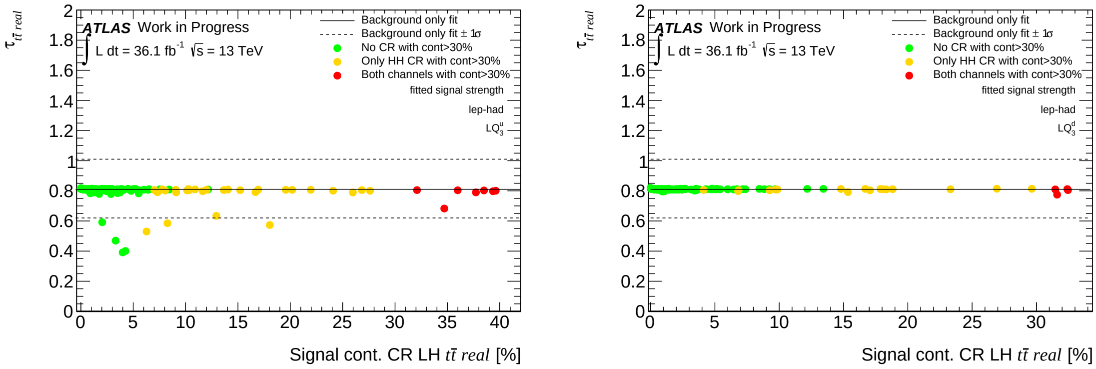

Figure 4.18: Same plots as in figure 4.16, but with the lep-had fit and $\mathrm{LQ}_3^{\mathrm{u}}$ on the left and $\mathrm{LQ}_3^{\mathrm{d}}$ on the right. (There is no CR for $t\bar{t}$ *fake* and no normalization factor for $t\bar{t}$ *fake* in the lep-had channel.)

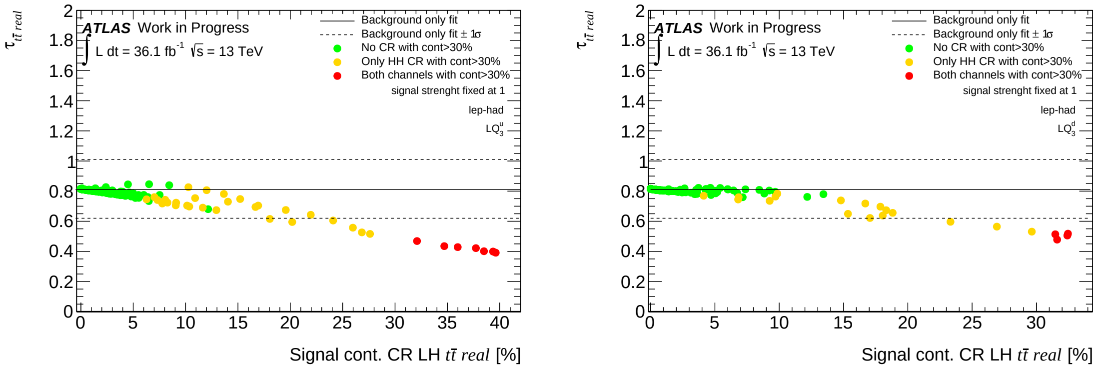

Figure 4.19: Same plots as in figure 4.18, but with fixed signal strengths.

4.5.3 Combined exclusion limits

Several ATLAS analysis teams worked together in order to determine combined exclusion limits for $\mathrm{LQ}_3^{\mathrm{u}}$ and $\mathrm{LQ}_3^{\mathrm{d}}$ with the same data considered in this work. All of these searches are reinterpretations and mostly of third generation SUSY searches:

- **stop 0L** The "stop 0L" analysis is a search for top squark pair production with final states containing jets and $E_{\mathrm{T}}^{\mathrm{miss}}$ [52].
- **stop 1L** The "stop 1L" analysis is a search for top squark pair production with final states containing one lepton, jets and $E_{\mathrm{T}}^{\mathrm{miss}}$ [53].
- **sbottom** The "sbottom" analysis is a search for SUSY in events with b-tagged jets and $E_{\mathrm{T}}^{\mathrm{miss}}$ [54].
- **di-Higgs** The "di-Higgs" analysis is a search for resonant and non-resonant di-Higgs production in the bb-$\tau\tau$ channel [55].

As we can see in figure 4.20, the analyses complement each other well. Without surprise, the di-Higgs search, which targets $bb\tau\tau$ final states, has high exclusion power in the region of high $\mathrm{BR}_{\mathrm{cl}}$. Analyses which require high $E_{\mathrm{T}}^{\mathrm{miss}}$ and jets (stop 0L, stop 1L and sbottom) are sensitive to the region of low $\mathrm{BR}_{\mathrm{cl}}$, where prompt neutrinos are frequent. The analysis presented in this work is the only one with its highest sensitivity in the region of intermediate values of $\mathrm{BR}_{\mathrm{cl}}$ and has a higher limit than all other analyses for $\mathrm{LQ}_3^{\mathrm{d}}$ with $\mathrm{BR}_{\mathrm{cl}}$ close to 0.5, the reason being that the analysis is most sensitive to mixed final states $t\tau b\nu$, as discussed in section 4.4. The lep-had channel of the stop-stau analysis is also the only one which requires a τ_{had}, a light lepton and $E_{\mathrm{T}}^{\mathrm{miss}}$.

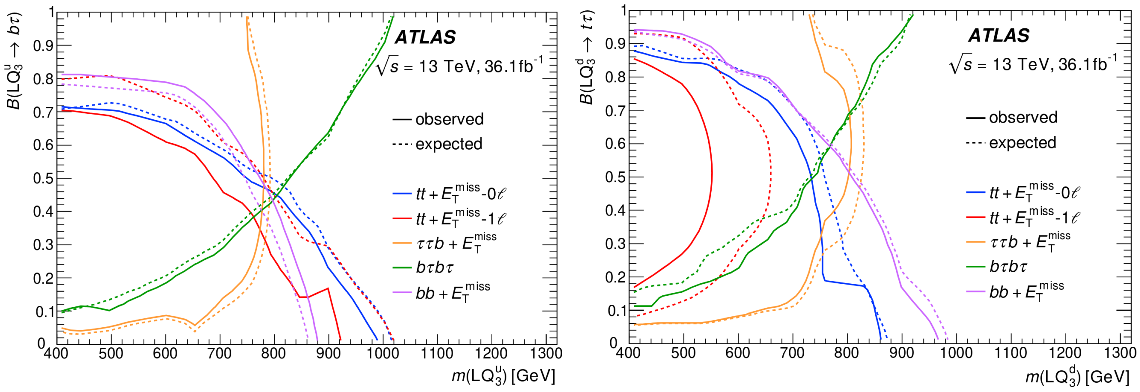

Figure 4.20: Observed and expected exclusion limits in the $\mathrm{BR}_{\mathrm{cl}}$-$m_{\mathrm{LQ}}$ plane at 95% CL of several reinterpretations of ATLAS searches for $\mathrm{LQ}_3^{\mathrm{u}}$ (left) and $\mathrm{LQ}_3^{\mathrm{d}}$ (right) [56]. The reinterpretation presented in this work is shown in orange.

4.5.4 Outlook

Further investigation is needed to understand the behavior of the fits with high signal contamination. In this work we chose not to exclude signals with high signal contamination and we defined an arbitrary limit of how much signal contamination is acceptable. This might be too conservative and the CL_s method may be applicable even in presence of high signal contamination.

Values of $\mathrm{BR}_{\mathrm{cl}}$ of 1 and 0 are easy to target, since the final state is always the same. For intermediate values of $\mathrm{BR}_{\mathrm{cl}}$, all three final states (with n_{cl}=0,1 and 2) are present. Nonetheless, we have seen that the stop-stau analysis is quite sensitive to intermediate values of $\mathrm{BR}_{\mathrm{cl}}$. It could be worthwhile to optimize a search for this region of $\mathrm{BR}_{\mathrm{cl}}$, based on the observations we made with this reinterpretation. In order to do this, it is clear that the main discriminating variable of the stop-stau analysis, m_{T2}, should be replaced or modified. Indeed, we only use the selected leptons to compute m_{T2}, since originally it should reconstruct the transverse masses of tau sleptons, which decay into a tau lepton and a neutrino. But for the leptoquark signal models, we should try to reconstruct the transverse masses of leptoquarks. Computing the transverse masses of the $b\nu$ and $b\tau$ systems would make more sense. The lepton requirements might also not be necessary. A selection of one tau lepton, b-jets and $E_{\mathrm{T}}^{\mathrm{miss}}$ could be a good channel to target LQ_3models with $\mathrm{BR}_{\mathrm{cl}}$=0.5.

Finally, we should not forget that we worked with simplified models, which are not identical to the theoretically motivated leptoquark states presented in table 2.3. The simplified models were built such that we have access to all possible final states emerging from pair produced third generation leptoquarks. But this is only true if we neglect the difference between particle and antiparticle, in the sense that we do not consider the difference between e.g. a leptoquark that couples to $\tau^- t$ (which corresponds to S_{1L} or S_{1R} in table 2.3) and a leptoquark that couples to $\tau^- \bar{t}$ (which corresponds to R_{2L} or R_{2R}). We would otherwise need additional simplified models, with different leptoquark charges. For a $\tau^- \bar{t}$ coupling, this would be $Q_{\mathrm{EM}} = \pm 5/3$. It is not clear to which extend the yields in the SRs would be affected by such an exchange. Our analysis requires the charges of the selected leptons to be of opposite sign (OS). One could think that, exchanging t with $\bar{t}$ does not have an impact on the result, since we consider production of the LQ and its antiparticle and intend to select an analogous lepton from each decay branch, such that the selected leptons are of opposite sign. But as we have discussed in section 4.4, we sometimes rely on the selection of a lepton from the decay of the top quark in the preselection, which can emerge from the decay of either LQ or $\overline{\mathrm{LQ}}$, such that the charges of the selected leptons are not fixed relative to eachother. With the simplified models used in this analysis, there were not many events left with same-sign leptons after applying all other SR cuts, as can be seen in figures 4.8 and 4.9. But this could be different for other simplified models. Determining the sensitivity of this analysis to the models that were not covered here, provides an interesting opportunity for an extension of the reinterpretation.

Chapter 5

Conclusion

We have reinterpreted the ATLAS search for top squarks decaying to tau sleptons in 36.1 fb^{-1} pp collisions at $\sqrt{s} = 13$ TeV [1] in terms of pair-produced third generation scalar leptoquarks of up-type ($\mathrm{LQ}_3^{\mathrm{u}}$) and down-type ($\mathrm{LQ}_3^{\mathrm{d}}$). We have shown that the analysis has good sensitivity for models in which leptoquarks decay into a charged lepton and a quark with branching ratios close to 0.5. We exclude $\mathrm{LQ}_3^{\mathrm{u}}$ masses up to 780 GeV and $\mathrm{LQ}_3^{\mathrm{d}}$ masses up to 800 GeV. Leptoquark signals have shown to yield much lower values of the main discriminating variable, the stransverse mass m_{T2}, compared to the stop-stau signals, which were targeted by the original analysis. This resulted in lower signal efficiencies in the signal regions and higher signal contamination in the control regions for $t\bar{t}$. Signal contamination challenged our ability to exclude some of the model's parameter space, but we were able to mitigate this effect by using one of the analysis channel separately.

Bibliography

[1] ATLAS Collaboration. *Search for top squarks decaying to tau sleptons in pp collisions at* $\sqrt{s}$*=13 TeV with the ATLAS detector*. arXiv:1803.10178 [hep-ex] (2018)

[2] Mark Thomson. *Modern Particle Physics*. University of Cambridge (2013).

[3] Howard Baer, Xerxes Tata. *Weak Scale Supersymmetry*. Cambridge university press (2006).

[4] Pierre Binétruy. *Supersymmetry*. Oxford university press (2006).

[5] Work by Wikipedia user MissMJ, citing PBS NOVA, Fermilab, Office of Science, United States Department of Energy, Particle Data Group en.wikipedia.org/wiki/Standard_Model.

[6] Work by Wikipedia user Eric Drexler. https://en.wikipedia.org/wiki/Standard_Model.

[7] Katherine Garrett and Gintaras Duda. *Dark Matter: A Primer*. arXiv:1006.2483 [hep-ph] (2011).

[8] P. J. E. Peebles, Bharat Ratra. *The Cosmological Constant and Dark Energy*. arXiv:astro-ph/0207347 (2002).

[9] *The 2004 nobel prize in physics - popular information*. N.M.A. 2014 (2017). https://www.nobelprize.org/nobel_prizes/physics/laureates/2004/popular.html.

[10] I.-A. Melzer-Pellmann, P.Pralavorio. *Lessons for SUSY from the LHC after the first run*. arXiv:1404.7191v3 [hep-ex] (2014).

[11] P. Lees et al. *Measurement of an Excess of* $\overline{B} \to D^{(*)}\tau^-\overline{\nu}_\tau$ *Decays and Implications for Charged Higgs Bosons*. arXiv:1303.0571 [hep-ex] (2013).

[12] Huschle et al. *Measurement of the branching ratio of* $\overline{B} \to D^{(*)}\tau^-\overline{\nu}_\tau$ *relative to decays* $D^{(*)}\ell^-\overline{\nu}_\ell$ *with hadronic tagging at Belle*. arXiv:1507.03233 [hep-ex] (2015).

[13] Aaij et al. *Measurement of the ratio of branching fractions* $\mathrm{B}(\overline{B}^0 \to D^{*+}\tau^-\nu_{\overline{\tau}})/\mathrm{B}(\overline{B}^0 \to D^{*+}\mu^-\nu_{\overline{\mu}})$. arXiv:1303.0571 [hep-ex] (2015).

[14] Ben Gripaios, M. Nardecchia, S. A. Renner. *Composite leptoquarks and anomalies in B-meson decays*. arXiv:1412.1791v2 [hep-ph] (2015).

[15] Jogesh C. Pati, Abdus Salam. *Lepton number as the fourth "color"*. Physical Review D vol.10 number 1, arXiv: 1203.0196v2 [hep-ph] (1974).

[16] A. V. Kuznetsov, N. V. Mikheev, A. V. Serghienko. *The third type of fermion mixing and indirect limits on the PatiSalam leptoquark mass*. International Journal of Modern Physics A, arXiv: 1203.0196v2 [hep-ph] (2012).

[17] Howard Georgi, S.L. Glashow *Unity of All Elementary-Particle Forces*. Physical Review Letters Vol32, 8 (1974).

[18] Howard Georgi. *Particles and Fields*. Proceeding of the APS Div. of Particles and Fields, ed. C. Carlson (1975).

[19] C. Patrignani et al. *Review of particle physics*. *Chin. Phys. C*, 40, 100001 (2016).

[20] David Bailey,Bruce A. Campbell. *Model independent constraints on leptoquarks from rare processes*. arXiv:hep-ph/9309310v1 (1993).

[21] Jose Wudka. *Composite Leptoquarks*. Physics Letters Vol 167B, number 3 (1986).

[22] Ben Gripaios. *Composite Leptoquarks at the LHC*. arXiv:0910.1789v3 [hep-ph] (2010).

[23] Barbara Schrempp, Fridger Schrempp. *Light Leptoquarks*. Physics Letters Vol 153B, number 1,2 (1985).

[24] Zhenjun Xiao. *Technicolor leptoquarks and the excess of NC and CC events with high-Q^2 at HERA*. arXiv:hep-ph/9709324v1 (1997).

[25] G. Altarelli. *HERA data and leptoquarks in supersymmetry*. arXiv:hep-ph/9708437v1 (1997).

[26] Joanne L. Hewett, Thomas G. Rizzo. *Much Ado About Leptoquarks: A Comprehensive Analysis*. Physical Review D (1997).

[27] Borut Bajc, Junji Hisano, Takumi Kuwahara, Yuji Omura. *Threshold Corrections to Dimension-six Proton Decay Operators in Non-minimal SUSY SU(5)GUTs*. arXiv:1603.03568v2 [hep-ph] (2016).

[28] Dominik Dannheim. *Searches for Flavour Changing Neutral Currents and Lepton Flavour Violation at HERA*. arXiv:hep-ex/0212004v1 (2002).

[29] Michael Krmer. *Pair production of scalar leptoquarks at the LHC*. arXiv:hep-ph/0411038v2 (2005).

[30] The CMS Collaboration. *Search for single production of scalar leptoquarks in proton-proton collisions at $\sqrt{s} = 8$ TeV*. arXiv:1509.03750v3 [hep-ex] (2016).

[31] Tanumoy Mandal,Subhadip Mitra,Satyajit Seth. *Pair Production of Scalar Leptoquarks at the LHC to NLO Parton Shower Accuracy*. arXiv:1506.07369v3 [hep-ph] (2016).

[32] The CMS Collaboration. *Search for pair production of first and second generation leptoquarks in proton-proton collisions at s = 8 TeV*. 10.1103/PhysRevD.93.032004 (2016).

[33] Education, Communications and Outreach Group. *LHC, the guide*. CERN-Brochure-2017-002-Eng.

[34] CERN. https://bigscience.web.cern.ch/bigscience/en/lhc/lhc2.html.

[35] Otmar Biebel. *Physics of Particle Detectors*. Lecture at LMU, Summer term 2016.

[36] ATLAS Collaboration *Detector and Technology* https://atlas.cern/discover/detector.

[37] The ATLAS Collaboration et al. *The ATLAS Experiment at the CERN Large Hadron Collider*. JINST 3 S08003 (2008).

[38] Zachary Marshall and the Atlas Collaboration. *Simulation of Pile-up in the ATLAS Experiment*. J. Phys.: Conf. Ser. 513 022024 (2014).

[39] Thomas Kuhr, Andreas Wildauer. *Physik der schweren Quarks.*. Lecture LMU, Summer term 2016.

[40] J. Pequenao and P. Schaffner. *An computer generated image representing how ATLAS detects particles*. https://cds.cern.ch/record/1505342 (2013).

[41] ATLAS Collaboration. *Reconstruction and identification of electrons in ATLAS*. ATLAS CSC Note EG-1.

[42] ATLAS Collaboration. *Muon identification algorithms in ATLAS*. Proceedings of science (2009).

[43] ATLAS Collaboration. *Selection of Jets Produced in 13 TeV Proton-Proton Collisions with the ATLAS Detector*. arXiv:0802.1189[hep-ph] (2015).

[44] A. Hrynevich. *ATLAS jet and missing energy reconstruction, calibration and performance in LHC Run-2*. JINST 12 C06038 (2017).

[45] ATLAS Collaboration. *Expected Performance of the ATLAS b-tagging Algorithms in Run-2*. ATL-PHYS-PUB-2015-022 (2015).

[46] ATLAS Collaboration. *Tau Lepton Reconstruction and Identification at ATLAS*. arXiv:1201.5466v1 [hep-ex] (2012).

[47] A. L. Read. *Presentation of search results: The CL(s) technique*. J. Phys. G, G28,26932704 (2012).

[48] J. Neyman, E.S.Pearson. *On the Problem of the Most Efficient Tests of Statistical Hypothesis*. Philosophical Transactions of the Royal Society A: Mathematical, Physical and Engineering Sciences. 231 (694706): 289337. (1933).

[49] E. Gross G. Cowan, K. Cranmer and O. Vitells. *Asymptotic formulae for likelihood-based tests of new physics*. Eur.Phys.J.C71:1554, arXiv:1007.1727 (2010,2011).

[50] M. Baak et al.. *HistFitter software framework for statistical data analysis*. Eur.Phys.J. C 75:153., 2015. arXiv:1410.1280 [hep-ex] (2015).

[51] Christoph Borschensky, Michael Krmer, Anna Kulesza, Michelangelo Mangano, Sanjay Padhi, Tilman Plehn, Xavier Portell. *Squark and gluino production cross sections in pp collisions at* $\sqrt{s} = 13$*, 14, 33 and 100 TeV*. Eur.Phys.J. C74, arXiv: 1407.5066v2 [hep-ph] (2014).

[52] ATLAS Collaboration. *Search for a scalar partner of the top quark in the jets plus missing transverse momentum final state at* $\sqrt{s}$*=13 TeV with the ATLAS detector*. arXiv:1709.04183 [hep-ex] (2017).

[53] ATLAS Collaboration. *Search for top-squark pair production in final states with one lepton, jets, and missing transverse momentum using 36.1 fb*$^{-1}$ *of* $\sqrt{s}$*=13 TeV pp collision data with the ATLAS detector*. arXiv:1711.11520 [hep-ex] (2017).

[54] ATLAS Collaboration. *Search for supersymmetry in events with b-tagged jets and missing transverse momentum in pp collisions at* $\sqrt{s}$*=13 TeV with the ATLAS detector*. arXiv:1708.09266 [hep-ex] (2017).

[55] ATLAS Collaboration. *Searches for resonant and non-resonant di-Higgs production in the bb-tautau decay channel in pp collisions at* $\sqrt{s}$*=13 TeV with the ATLAS detector*. arXiv:1708.09266 [hep-ex] (2017).

[56] ATLAS Collaboration. *Searches for third-generation scalar leptoquarks in* $\sqrt{s}$*=13 TeV pp collisions with the ATLAS detector*. arXiv:1902.08103 [hep-ex] (2019).

[57] ATLAS Collaboration. *Search for direct top squark pair production decaying in final states with two tau leptons in pp collisions at* $\sqrt{s}$*=8 TeV with the ATLAS detector*. arXiv:1509.04976v2 [hep-ex] (2016).

[58] Lorenzo Moneta et al. *The RooStats Project*. arXiv:1009.1003 [physics.data-an] (2010).

Appendix A

A.1 Signal region optimization for the lep-lep channel of the stop-stau analysis

A signal region optimization was done for the lepton-lepton channel to see if it could contribute to the exclusion power of the analysis. In the stop-stau Run-1 analysis [57], the lep-lep channel was able to contribute in compressed scenarios ($m(\tilde{t})$ close to $m(\tilde{\tau})$), where the other channels lacked sensitivity. So the goal of this study is to see if we can repeat this for Run-2. The preselection for this channel is shown in table A.1.

Preselection cuts lep-lep
exactly 2 light leptons
trigger requirements: cut on lepton p_T

Table A.1: Preselection for the lep-lep channel

The same trigger strategy as in the lep-had channel was used. An additional dilepton trigger could potentially enhance the statistics for this channel by including events for which the leading lepton has a smaller transverse momentum than the plateau cuts of the single electron and single muon triggers. But, as can be seen from figure A.1, the distribution of the transverse momentum of the leading lepton suggests that the amount of concerned events is rather small.
A brute-force scan of multiple cut combinations is performed to design a signal region, which aims to optimize the signal-to-background ratio, but still has a reliable MC background estimate, which means that we required at least one total background event and one raw event for each background to pass the selection. Four signal regions were optimized for four different benchmark points, namely the points with $(m(\tilde{t}), m(\tilde{\tau}))$ taking the values $(600, 590)$, $(800, 840)$, $(1000, 990)$ and $(1000, 990)$ GeV.

The initial set of variables used in the optimization is:

$$\begin{gathered} E_{\mathrm{T}}^{\mathrm{miss}},\ m_{\mathrm{T2}}(\ell,\ell),\ m_{\mathrm{eff}}(\ell,\ell),\ m(\ell,\ell),\ m_{\mathrm{T}}^{\mathrm{sum}}(\ell,\ell),\ p_{\mathrm{T}}(\ell_{1,2}),\ p_{\mathrm{T}}(\mathrm{j}_{1,2}), \\ \Delta\phi_{\mathrm{min}}(\mathrm{j}_{1,2}, E_{\mathrm{T}}^{\mathrm{miss}}),\ \Delta\phi(\ell_1, E_{\mathrm{T}}^{\mathrm{miss}}),\ H_{\mathrm{T}},\ n_{b\text{-jets}},\ n_{\tau},\ n_{\mathrm{j}},\ \Delta\phi_b, \end{gathered} \tag{A.1}$$

where $\Delta\phi_b$ is the the azimuthal angular distance between $\mathbf{E}_{\mathrm{T}}^{\mathrm{miss}}$ and $\mathbf{E}_{\mathrm{T}}^{\mathrm{miss}} + \mathbf{p}_{\mathrm{T}}(\ell_1) + \mathbf{p}_{\mathrm{T}}(\ell_2)$. $\Delta\phi_{\mathrm{min}}(\mathrm{j}_{1,2}, E_{\mathrm{T}}^{\mathrm{miss}})$ is the minimal angle between either of the first two leading jets and $E_{\mathrm{T}}^{\mathrm{miss}}$ and $\Delta\phi(\ell_1, E_{\mathrm{T}}^{\mathrm{miss}})$ is the angle between the leading lepton and $E_{\mathrm{T}}^{\mathrm{miss}}$. All other variables are the same as described in section 4.2, but applied to the two selected light leptons.
The optimized signal regions are summarized in table A.2, a scan on the significance for each

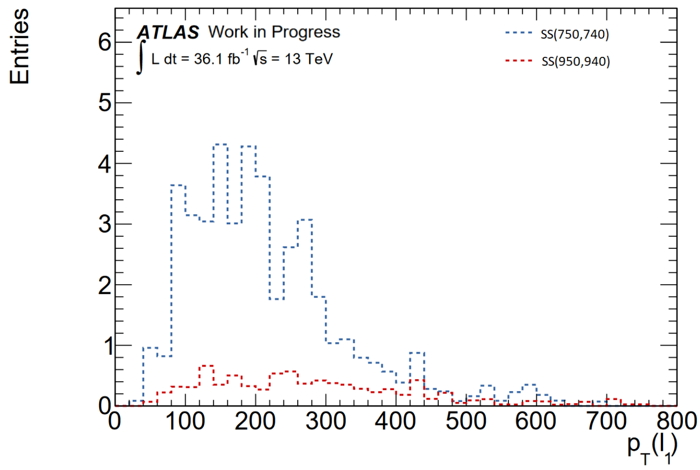

Figure A.1: Transverse momentum of the leading lepton with the lep-lep preselection for stop-stau signals with $(m(\tilde{t}), m(\tilde{\tau})) = (750, 740)$ and $(950, 940)$.

mass point and signal region is shown in figure A.2. The significance Z is calculated with the RooStats-package [58] with a relative uncertainty on the background of 30%.

The lep-lep signal regions designed in this study are not sensitive to a region not already covered by the other channels.

Variable	$(600, 590)$	$(850, 840)$	$(1000, 990)$	$(900, 490)$
$\text{sign}(\ell, \ell)$	OS	OS	OS	OS
$E_{\text{T}}^{\text{miss}}$	> 250 GeV	> 250 GeV	> 250 GeV	> 290 GeV
$m_{\text{T2}}(\ell, \ell)$	> 120 GeV	> 120 GeV	> 120 GeV	> 100 GeV
$m(\ell, \ell)$	> 180 GeV	> 210 GeV	> 190 GeV	> 120 GeV
$p_{\text{T}}(\ell_1)$	> 90 GeV	> 160 GeV	> 170 GeV	> 90 GeV
$p_{\text{T}}(\ell_2)$	> 70 GeV	> 90 GeV	> 120 GeV	—
$p_{\text{T}}(\text{j}_1)$	< 300 GeV	< 600 GeV	< 500 GeV	—
$p_{\text{T}}(\text{j}_2)$	< 100 GeV	< 200 GeV	< 200 GeV	—
n_{τ}	0	0	0	0
n_{j}	< 7	< 6	< 6	> 1
$n_{b\text{-jets}}$	—	—	—	> 0
$\Delta\phi_b$	< 1.4	< 1.8	< 1.7	< 1.4
H_{T}	—	—	—	> 240 GeV

Table A.2: Signal regions in the leplep channel, optimized for $(m(\tilde{t}), m(\tilde{\tau})) = (600, 590)$, $(800, 840)$, $(1000, 990)$ and $(900, 490)$ (GeV)

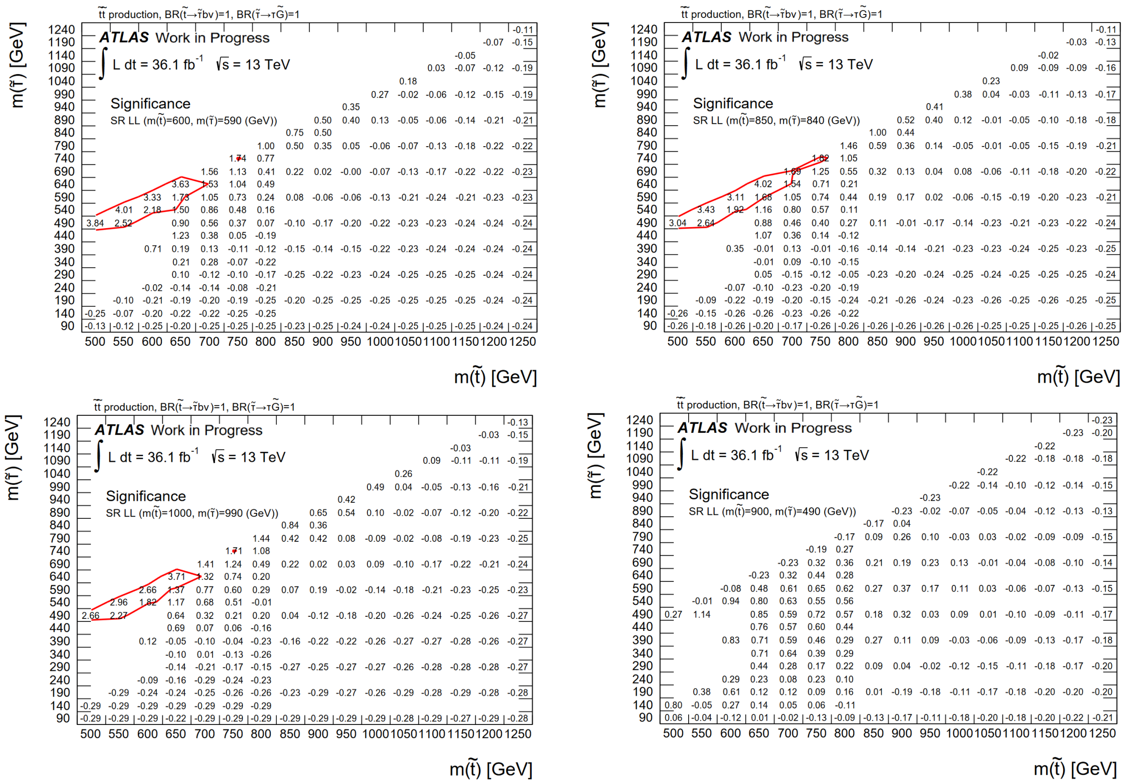

Figure A.2: Significances computed with a fixed uncertainty of 30% on the total background. The red line circles values of 1.64, such that it would contain excluded models at 95% CL. The SRs are optimized for $(m(\tilde{t}), m(\tilde{\tau})) = (600, 590)$ (top-left), $(800, 840)$ (top-right), $(1000, 990)$ (bottom-left) and $(900, 490)$ (bottom-right) (GeV).

A.2 Leptoquark signal samples

DSID	type/ M_{LQ} [GeV]	sample name	σ [pb]	$\Delta\sigma$ [%]	$\hat{\mathrm{BR}}_{cl}$
309085	up/400	aMcAtNloPy8EG_A14N30NLO_LQ3_up_beta05_M400	1.835	±13.698	0.601
309086	up/500	aMcAtNloPy8EG_A14N30NLO_LQ3_up_beta05_M500	0.518	±13.38	0.563
309087	up/600	aMcAtNloPy8EG_A14N30NLO_LQ3_up_beta05_M600	0.175	±13.207	0.543
309088	up/650	aMcAtNloPy8EG_A14N30NLO_LQ3_up_beta05_M650	0.107	±12.923	0.536
309089	up/700	aMcAtNloPy8EG_A14N30NLO_LQ3_up_beta05_M700	0.067	±13.343	0.531
309090	up/750	aMcAtNloPy8EG_A14N30NLO_LQ3_up_beta05_M750	0.043	±13.745	0.527
309091	up/800	aMcAtNloPy8EG_A14N30NLO_LQ3_up_beta05_M800	0.028	±14.171	0.524
309092	up/850	aMcAtNloPy8EG_A14N30NLO_LQ3_up_beta05_M850	0.019	±14.702	0.521
309093	up/900	aMcAtNloPy8EG_A14N30NLO_LQ3_up_beta05_M900	0.013	±15.203	0.519
309094	up/1000	aMcAtNloPy8EG_A14N30NLO_LQ3_up_beta05_M1000	0.006	±16.295	0.515
309502	up/950	aMcAtNloPy8EG_A14N30NLO_LQ3_up_beta05_M950	0.009	±15.718	0.517
309503	up/1050	aMcAtNloPy8EG_A14N30NLO_LQ3_up_beta05_M1050	0.004	±16.786	0.514
309504	up/1100	aMcAtNloPy8EG_A14N30NLO_LQ3_up_beta05_M1100	0.003	±17.473	0.512
309095	down/400	aMcAtNloPy8EG_A14N30NLO_LQ3_down_beta05_M400	1.835	±13.698	0.399
309096	down/500	aMcAtNloPy8EG_A14N30NLO_LQ3_down_beta05_M500	0.518	±13.38	0.437
309097	down/600	aMcAtNloPy8EG_A14N30NLO_LQ3_down_beta05_M600	0.175	±13.207	0.457
309098	down/650	aMcAtNloPy8EG_A14N30NLO_LQ3_down_beta05_M650	0.107	±12.923	0.464
309099	down/700	aMcAtNloPy8EG_A14N30NLO_LQ3_down_beta05_M700	0.067	±13.343	0.469
309100	down/750	aMcAtNloPy8EG_A14N30NLO_LQ3_down_beta05_M750	0.043	±13.745	0.473
309101	down/800	aMcAtNloPy8EG_A14N30NLO_LQ3_down_beta05_M800	0.028	±14.171	0.476
309102	down/850	aMcAtNloPy8EG_A14N30NLO_LQ3_down_beta05_M850	0.019	±14.702	0.479
309103	down/900	aMcAtNloPy8EG_A14N30NLO_LQ3_down_beta05_M900	0.013	±15.203	0.481
309104	down/1000	aMcAtNloPy8EG_A14N30NLO_LQ3_down_beta05_M1000	0.006	±16.295	0.485
309505	down/950	aMcAtNloPy8EG_A14N30NLO_LQ3_down_beta05_M950	0.009	±15.718	0.483
309506	down/1050	aMcAtNloPy8EG_A14N30NLO_LQ3_down_beta05_M1050	0.004	±16.786	0.486
309507	down/1100	aMcAtNloPy8EG_A14N30NLO_LQ3_down_beta05_M1100	0.003	±17.473	0.488

Table A.3: Dataset IDs (DSID), LQ3 masses and sample names, LQ3 production cross-sections and their uncertainties and branching ratios into charged leptons of the samples used.

Selbständigkeitserklärung

Hiermit erkläre ich, die vorliegende Arbeit selbständig verfasst zu haben und keine anderen als die in der Arbeit angegebenen Quellen und Hilfsmittel benutzt zu haben.

München, 09.05.2018

Alexander Mario Lory